The senescent secretome drives PLVAP expression in cultured human hepatic endothelia to promote monocyte transmigration

Wilkinson, Alex L.; Hulme, Samuel; Kennedy, James I.; Mann, Emily R.; Horn, Paul; Shepherd, Emma L.; Yin, Kelvin; Zaki, Marco Y.W.; Hardisty, Gareth; Lu, Wei-Yu; Rantakari, Pia; Adams, David H.; Salmi, Marko; Hoare, Matthew; Patten, Daniel A.; Shetty, Shishir

DOI:
10.1016/j.isci.2023.107966

Journal Pre-proof

The senescent secretome drives PLVAP expression in cultured human hepatic endothelia to promote monocyte transmigration

Alex L. Wilkinson, Samuel Hulme, James I. Kennedy, Emily R. Mann, Paul Horn, Emma L. Shepherd, Kelvin Yin, Marco Y.W. Zaki, Gareth Hardisty, Wei-Yu Lu, Pia Rantakari, David H. Adams, Marko Salmi, Matthew Hoare, Daniel A. Patten, Shishir Shetty

PII: S2589-0042(23)02043-6

DOI: https://doi.org/10.1016/j.isci.2023.107966

Reference: ISCI 107966

To appear in: *ISCIENCE*

Received Date: 27 March 2023

Revised Date: 31 May 2023

Accepted Date: 15 September 2023

Please cite this article as: Wilkinson, A.L., Hulme, S., Kennedy, J.I., Mann, E.R., Horn, P., Shepherd, E.L., Yin, K., Zaki, M.Y.W., Hardisty, G., Lu, W.-Y., Rantakari, P., Adams, D.H., Salmi, M., Hoare, M., Patten, D.A., Shetty, S., The senescent secretome drives PLVAP expression in cultured human hepatic endothelia to promote monocyte transmigration, *ISCIENCE* (2023), doi: https://doi.org/10.1016/j.isci.2023.107966.

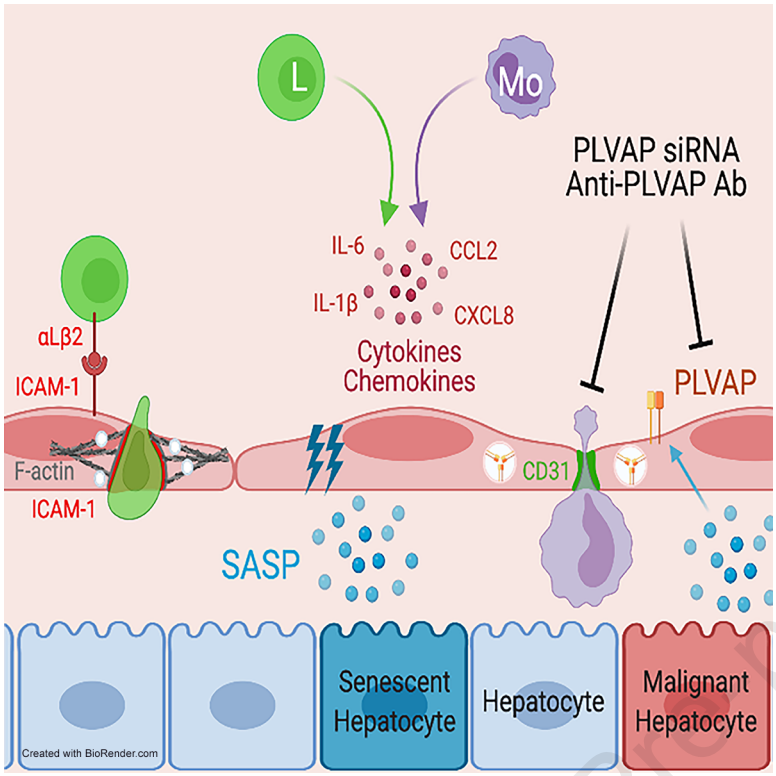

The senescent secretome drives PLVAP expression in cultured human hepatic endothelia to promote monocyte transmigration

Alex L. Wilkinson[1], Samuel Hulme[1], James I. Kennedy[1], Emily R. Mann[1], Paul Horn[1], Emma L. Shepherd[1], Kelvin Yin[2], Marco Y. W. Zaki[3], Gareth Hardisty[4], Wei-Yu Lu[4], Pia Rantakari[5, 6], David H. Adams[1], Marko Salmi[5, 6], Matthew Hoare[2,7], Daniel A. Patten[1,8†] and Shishir Shetty[1,8,9*†]

[1] *Centre for Liver and Gastrointestinal Research, Institute of Immunology and Immunotherapy, University of Birmingham, Birmingham, B15 2TT, United Kingdom*

[2]*University of Cambridge, Cancer Research UK Cambridge Institute, Robinson Way, Cambridge CB2 0RE, United Kingdom*

[3]*Department of Biochemistry, Faculty of Pharmacy, Minia University, Egypt*

[4]*Centre for Inflammation Research, University of Edinburgh*

[5]*Institute of Biomedicine, University of Turku, Turku, Finland*

[6]*MediCity Research Laboratory, University of Turku, Turku, Finland*

[7]*University of Cambridge, Department of Medicine, Addenbrooke's Hospital, Cambridge CB2 0QQ, United Kingdom*

[8]*National Institute for Health Research Biomedical Research Centre at University Hospitals Birmingham NHS Foundation Trust, University of Birmingham, Birmingham, UK.*

[9]*Lead contact*

†equal senior authorship

***Corresponding author**:
Prof Shishir Shetty
National Institute for Health Research Birmingham Liver Biomedical Research Unit and Centre for Liver Research
Institute of Immunology and Immunotherapy
University of Birmingham
Birmingham
B15 2TT
United Kingdom
Email: s.shetty@bham.ac.uk
Tel: +44 121 415
Fax: +44 121 415 8701

Keywords: Senescence, PLVAP, Liver Endothelium, Monocyte

Summary

Liver sinusoidal endothelial cells (LSEC) undergo significant phenotypic change in chronic liver disease (CLD) and yet the factors that drive this process and the impact on their function as a vascular barrier and gatekeeper for immune cell recruitment are poorly understood. Plasmalemma vesicle-associated protein (PLVAP) has been characterised as a marker of LSEC in CLD, notably we found that PLVAP upregulation strongly correlated with markers of tissue senescence. Furthermore, exposure of human LSEC to the senescence associated secretory phenotype (SASP) led to a significant upregulation of PLVAP. Flow based assays demonstrated that SASP-driven leukocyte recruitment was characterised by paracellular transmigration of monocytes whilst the majority of lymphocytes migrated transcellularly. Knockdown studies confirmed that PLVAP selectively supported monocyte transmigration mediated through PLVAP's impact on LSEC permeability by regulating Phospho-VE-cadherin expression and endothelial gap formation. PLVAP may therefore represent an endothelial target which selectively shapes the senescence-mediated immune microenvironment in liver disease.

Introduction

Chronic liver disease (CLD) is a global health burden accounting for approximately two million deaths/year worldwide[1, 2]. Ranking the second most common cause of premature death in the UK, CLD is also a major risk factor for developing hepatocellular carcinoma (HCC), which is predicted to affect >1 million individuals per year globally by 2025[2-4]. CLDs are characterised by leukocyte infiltration which drives chronic inflammation and fibrosis independently of aetiology. The recruitment of immune cells takes place within the hepatic sinusoids which are lined by highly specialised fenestrated endothelia that act as the liver gatekeepers[5, 6]. The distinct phenotype of liver sinusoidal endothelial cells (LSEC), paired with the low shear environment within the hepatic sinusoids, fosters a unique environment in which leukocyte recruitment can occur. As such, it has become clear that the mechanisms which mediate this recruitment in the liver are distinct from more conventional vascular beds; understanding this process is critical to identify novel therapeutic targets which could allow selective manipulation of the hepatic immune microenvironment in CLD to promote wound healing and reduce cancer risk.

Plasmalemma vesicle-associated protein (PLVAP) is the antigen recognised by PAL-E (Pathologische Anatomie Leiden-endothelium) and MECA-32 (mouse endothelial cell antigen-32) antibodies used to identify vascular endothelium in human and mouse tissues, respectively[7, 8]. It has long been considered an endothelial-specific protein, forming homodimeric diaphragms which span the openings of fenestrae and caveolae[9-11]. In addition to its role in development, vascular permeability and angiogenesis, as a component of these diaphragms, several studies have also implicated PLVAP in leukocyte trafficking[12-14]. In particular, one study identified that PLVAP in lymphatic endothelium is important for lymphocyte entry into the lymph nodes[13], whilst another study indicated that PLVAP is integral for the egress of foetal liver monocytes and subsequent seeding as tissue-resident macrophages during development[14].

Notably, recent single-cell RNA sequencing studies in humans have highlighted the re-emergence of PLVAP in diseased endothelium, such as within scar-associated endothelia of cirrhotic patients[15] and tumour endothelia of HCC patients[16]. Despite this, the regulation and functional role of PLVAP in liver disease is still poorly understood. Here, we confirmed that PLVAP is indeed upregulated in human liver cirrhosis, but for the first time, to our knowledge, demonstrate a direct correlation with cellular senescence within liver tissue.

In the context of both CLD and HCC, hepatocytes have previously been shown to reside in a state of cellular senescence[17], a process associated with production of a distinct secretome known as the senescence-associated secretory phenotype (SASP). The SASP has been characterised to comprise numerous cytokines, chemokines, growth factors, extracellular matrix proteins and extracellular vesicles that are important in shaping the senescence tissue microenvironment[18]. Importantly, the SASP is thought to drive recruitment of leukocytes to facilitate clearance of pre-

malignant senescent cells, and indeed previous work suggests that monocytes and $CD4^+$ T lymphocytes are critical in this process[19, 20]. We have previously demonstrated that SASP-stimulated liver endothelial cells support recruitment of peripheral blood lymphocytes under physiological shear conditions[21], but the molecular mechanisms of SASP-mediated leukocyte recruitment have yet to be completely elucidated. Here, we demonstrate that monocytes and lymphocytes transmigrate across SASP-stimulated LSEC using distinct pathways, identifying a specific role for PLVAP in monocyte recruitment. Furthermore, we utilise RNA sequencing, immunostaining and transendothelial electrical resistance (TEER) assays to show that PLVAP supports paracellular migration by altering endothelial junctional integrity.

Results

PLVAP is upregulated within scar-associated endothelium in a range of human chronic liver diseases

Analysis of *PLVAP* mRNA in whole tissue lysates from normal and cirrhotic liver demonstrated a 6.9-fold upregulation of *PLVAP* gene expression across several CLDs, including alcoholic liver disease (ALD), non-alcoholic steatohepatitis (NASH), primary biliary cholangitis (PBC) and primary sclerosing cholangitis (PSC) (**Figure 1A**). Quantification of PLVAP staining confirmed its significant upregulation (3.5-fold), which occurred in CLD, irrespective of the liver aetiology (**Figure 1B**). Furthermore, a positive correlation was observed between PLVAP and collagen deposition, as measured by Sirius red staining, in serial liver sections from the same patient (**Figure 1C**). Western blot analysis with an anti-PLVAP antibody detected a single band of ~30 kDa which was largely absent from normal liver but significantly increased (7.9-fold) in CLD samples (**Supplementary Figure 1A**). Immunohistochemical staining demonstrated that $PLVAP^+$ vessels localised within fibrotic tracts (visualised using Sirius red) and also in the peri-fibrotic sinusoids (**Figure 1D, Supplementary Figure 1B**).

We next performed further spatial and phenotypic characterisation of the $PLVAP^+$ cell population by dual immunofluorescent staining with endothelial and sinusoidal markers. In cirrhotic liver, PLVAP co-localised with classical vascular marker, CD31, whilst displaying a mutually exclusive expression pattern with proteins enriched in LSEC, including liver/lymph node-specific intercellular adhesion molecule-3-grabbing integrin (L-SIGN) and lymphatic vessel endothelial hyaluronan receptor 1 (LYVE-1) (**Figure 1E, Supplementary Fig 2A**). These data were in keeping with previous single-cell sequencing studies, highlighting an enrichment of *PLVAP* gene expression in endothelial cells which display a scar-associated genetic signature (**Supplementary Figure 2B**)[15]. Consistent with our findings, publicly-available single-cell sequencing data showed endothelial expression of *CLEC4M* (L-SIGN) and *LYVE1* in cells annotated as LSEC, in which *PLVAP* was largely absent (**Supplementary Figure 2C,D**). Moreover, *PLVAP* was often co-expressed with *PECAM1* (CD31)

in cirrhotic human liver endothelium (**Supplementary Figure 2C,D**). Collectively, these data confirm that PLVAP is upregulated in human CLD and suggest that it defines a distinct scar-associated endothelial cell subset that may contribute to disease pathogenesis.

PLVAP correlates with senescence and immune infiltrate in CLD and is upregulated by the senescent secretome

Previous studies have shown that hepatocytes peripheral to fibrotic tracts in CLD tissues largely exist in a senescent state[22-25]. Given that PLVAP is enriched within these same regions, we sought to investigate a potential link between PLVAP expression and hepatic senescence. Immunohistochemistry was performed on serial liver sections from the same patient to visualise PLVAP in conjunction with fibrotic regions (Sirius red), along with senescence markers, p21 and p16 (**Figure 2A**). From our immunohistochemical staining we could clearly identify $p21^+$ hepatocytes and found a significant increase in $p21^+$ hepatocytes in CLD compared to normal liver, quantified by positive cell per field of view (**Supplementary Figure 3A, B**). We also noted that the enrichment of PLVAP within peri-fibrotic areas spatially coincided with $p21^+$ hepatocytes (**Figure 2A**). In contrast, we found p16 staining was highly variable in cirrhotic specimens (**Supplementary Figure 3A, B**). $p16^+$ hepatocytes staining was relatively more homogenous in their distribution throughout regenerative nodules, localisation of other $p16^+$ cells (possibly immune cells) was observed within fibrotic septa in close association with PLVAP-enriched areas (**Figure 2A**) with total expression quantified as % area. Further analysis demonstrated that PLVAP was directly proportional to expression of p21 and p16 in matched human liver samples, at both the gene and the protein level, as determined by qRT-PCR (**Figure 2B**) and quantification of immunohistochemical staining (**Figure 2C**), respectively. These data highlight a previously unreported link between PLVAP expression and a senescent hepatic microenvironment in CLD.

Senescent cells release a secretome known as the senescence-associated secretory phenotype (SASP), which can regulate the immune microenvironment by driving leukocyte recruitment[19, 21, 26]. Given the distribution of $PLVAP^+$ endothelial cells within peri-fibrotic areas, which are frequent sites of leukocyte recruitment during chronic inflammation, we hypothesised that PLVAP could be a critical link between senescence and the immune microenvironment within the liver. We undertook immunohistochemistry of serial liver sections to visualise PLVAP with respect to immune cell infiltration; specifically, infiltrating monocytes (MAC387), T lymphocytes (CD3) and B lymphocytes (CD20) were explored. MAC387 is known to recognise both monocytes and neutrophils[27-29], and so neutrophil elastase (NE) staining was performed in matched cases. The levels of infiltrating neutrophils were minimal in all cases tested suggesting their contribution to MAC387-positivity was negligible (**Supplementary Figure 3C**). In normal liver, lymphocyte infiltration was minimal, whilst $MAC387^+$ cells were found to be homogenously distributed throughout the sinusoids (**Supplementary Figure 3D**). In contrast, in cirrhotic liver, PLVAP-rich areas marked the sites of

extensive MAC387$^+$, CD3$^+$ and CD20$^+$ cell infiltration (**Figure 2D**). Moreover, PLVAP (% area) positively correlated with MAC387 and CD3 (but not CD20) immunostaining in matched patient samples (**Figure 2E**), suggesting PLVAP may be associated with recruitment of monocytes and T lymphocytes in CLD.

***PLVAP expression is maintained in primary human LSEC and is upregulated by the senescent secretome* in vitro**

To investigate whether PLVAP expression is maintained *in vitro*, primary LSEC were isolated and *PLVAP* gene expression was compared to other cultured non-parenchymal hepatic cell types. *PLVAP* mRNA levels were significantly higher in LSEC when compared with activated liver myofibroblasts (aLMF) (>2000-fold), hepatic stellate cells (HSC) (7400-fold) and biliary epithelial cells (BEC) (4700-fold) (**Figure 3A**). The expression of PLVAP was also maintained *in vitro* at the protein level in passaged LSEC, as determined by immunofluorescence (**Figure 3B**). Notably, PLVAP was expressed only in a subset of LSEC, recapitulating observations *in situ* in human cirrhotic liver. In these positive LSEC, PLVAP often localised towards the cell periphery, although it was excluded from the VE-cadherin$^+$ intercellular junctions (**Figure 3B**).

As PLVAP expression was maintained in LSEC *in vitro* this offered the opportunity to study the regulation of PLVAP expression in these cells. Given the distinct spatial localisation of PLVAP relative to fibrotic septa, there are likely factors released and concentrated within these regions that are important for its paracrine regulation. As such, we developed a high-content imaging assay to probe the modulation of PLVAP in primary human LSEC in response to various stimuli (**Supplementary Figure 4A**). To confirm the sensitivity and validity of this assay we initially treated LSEC with tumour necrosis factor α (TNFα), which is known to upregulate intercellular adhesion molecule 1 (ICAM1) in liver endothelial cells in a dose-dependent manner[30] (**Supplementary Figure 4B, C**). Once optimised, the assay was repeated with vascular endothelial growth factor (VEGF), which has been shown to regulate PLVAP expression in multiple endothelial cell types[31-35]. Our assay confirmed that PLVAP expression was upregulated in human LSEC by vascular endothelial growth factor (VEGF) treatment for 24 hours, demonstrated by an increase in immunofluorescence area (1.8-fold ± 0.14) and intensity (1.9-fold ± 0.17) compared to the untreated control (**Supplementary Figure 4D, E**).

Building on these regulation studies, we next explored factors that more accurately reflect the liver microenvironment *in vivo*. VEGF plays an important role in angiogenesis and is a master regulator of endothelial cell biology, yet is also known to be a key mediator in CLD and HCC[36, 37]. Hepatocytes are known to be a major source of VEGF within the liver[38-40], and we confirmed that a hepatocyte-endothelial axis could be important for PLVAP regulation in CLD, showing that supernatants from hepatocyte cell line, HepG2, also upregulated PLVAP in LSEC (**Supplementary Figure 4F,G**).

Given the correlation between PLVAP and senescence in CLD specimens, paired with the regulatory effects of VEGF and hepatoma cell supernatants, we aimed to model a senescent microenvironment *in vitro*. We used a well-established and validated model of oncogene-induced senescence, in which SASP was obtained from IMR90 human diploid fibroblasts overexpressing tamoxifen-inducible oncogenic *HRAS*^{G12V} (Ras-CM), and compared this to the effects of the growing, non-senescent cell control ("Grow-CM"). This model has provided key insights into cellular senescence within the liver (21). Ras-CM stimulation of LSEC for 24 hours induced both PLVAP mRNA (3.0-fold) (**Figure 3C**) and protein expression (**Figure 3D, E**), significantly increasing immunofluorescence area (2.1-fold ± 0.19) and intensity (2.0-fold ± 0.34) in cultured LSEC. These data indicate that soluble factors released within a diseased tissue microenvironment may underpin the distinct expression of PLVAP.

The senescent secretome drives recruitment of lymphocytes and monocytes by molecularly distinct mechanisms

SASP release is known to facilitate senescent cell surveillance by driving immune cell recruitment[19, 21], and recently we have shown that LSEC play a critical role in this process[41]. Here, we confirm that primary human LSEC undergo activation in response to 24-hour Ras-CM treatment, including morphological changes such as elongation, cytoskeletal rearrangement and actin stress fibre formation (**Supplementary Figure 5A, B**), and production of proinflammatory cytokines, chemokines and adhesion molecules (**Supplementary Figure 5C-E**). We have previously shown that SASP-stimulated liver endothelial cells support lymphocyte recruitment under physiological shear stress[21]. To investigate whether SASP treatment can also drive monocyte recruitment *in vitro*, flow adhesion assays were performed with Grow-CM- or Ras-CM-stimulated LSEC and purified healthy peripheral blood monocytes. These flow based adhesion assays imaged with phase contrast microscopy recapitulate leukocyte recruitment within the hepatic sinusoids and permit analysis of each step of the adhesion cascade from leukocyte capture through to transendothelial migration[42-44] Monocyte adhesion (3.3-fold), shape-change (activation) (3.1-fold) and transmigration (7.7-fold) was significantly higher following LSEC SASP exposure compared to control cells (**Figure 4A, B**). Therefore, SASP-stimulated liver endothelial cells are capable of recruiting both lymphocytes and monocytes under physiologically low shear conditions.

Next, we studied the mechanisms of innate versus adaptive immune cell recruitment in response to the SASP, with a focus on myeloid and lymphocyte populations since their infiltration into the liver is a hallmark of several CLDs. High-resolution imaging of fluorescently-labelled LSEC by confocal microscopy revealed that SASP-primed monocyte and lymphocyte transmigration occurred via distinct endothelial routes. Specifically, >92% of monocytes transmigrated via the paracellular route in response to the SASP, which was determined by displacement of the VE-cadherin^{+} endothelial junctions (**Figure 4C**). In contrast, lymphocytes predominantly utilised the transcellular path (~60%) during transmigration, in association with F-actin-rich transmigratory pores (**Figure 4C**).

In keeping with the differences in transmigratory route, SASP-mediated monocyte and lymphocyte recruitment were also found to be molecularly distinct. Antibody-mediated ICAM1 blockade had no observed effect on monocyte recruitment but reduced both lymphocyte adhesion (0.7-fold ± 0.08) and % transmigration (from 41.0% to 30.6%) (**Figure 4D**). Furthermore, monocyte % transmigration was significantly impaired (from 32.6% to 19.8%) following antibody-mediated CD31 inhibition, whilst monocyte and lymphocyte adhesion were unaffected by CD31 blockade (**Figure 4E**). Lymphocyte transmigration was slightly reduced in CD31-inhibited LSEC, from 39.4% to 32%, although this was not statistically significant (**Figure 4E**). Consistent with these findings, transmigrating lymphocytes and monocytes were observed to associate with ICAM1 and CD31, respectively, during SASP-mediated recruitment (**Figure 4F, G**). Thus, the senescent secretome drives endothelial recruitment of monocytes and lymphocytes by distinct molecular mechanisms.

PLVAP contributes to SASP-mediated monocyte, but not lymphocyte, transmigration across primary human LSEC

Our next aim was to explore the functional contribution of PLVAP to hepatic leukocyte recruitment, as our earlier findings suggested a link between PLVAP, senescence and immune cell infiltration in CLD (**Figure 2**). Moreover, PLVAP has previously been implicated as a leukocyte trafficking molecule both *in vitro* and *in vivo*[12-14], thus, we sought to investigate a potential role for PLVAP in SASP-mediated innate/adaptive immune cell recruitment. Flow adhesion assays were performed following PLVAP inhibition in LSEC, either by genetic knockdown or antibody-mediated blockade, and the effects on recruitment of monocytes and lymphocytes were assessed (**Figure 5**). Transient siRNA transfection of LSEC resulted in robust knockdown of PLVAP mRNA (>95% efficiency) and protein (comparable to IMC) levels, as determined by qRT-PCR and high-content imaging, respectively (**Figure 5A**). Following siRNA knockdown of PLVAP, we demonstrated that whilst SASP-mediated monocyte adhesion was unaffected, there was a significant reduction of monocyte transendothelial migration (**Figure 5B**). This role appeared to be specific for monocytes, since flow adhesion assays with lymphocytes demonstrated no significant effect on adhesion or transmigration, following PLVAP knockdown (**Figure 5B**).

To validate our PLVAP knockdown findings, we undertook experiments with LSEC following antibody-mediated blockade of PLVAP. Treatment of live LSEC with an anti-PLVAP antibody indicated successful binding within 30 minutes (**Figure 5C**). Following antibody-mediated PLVAP blockade, no inhibition of lymphocyte transmigration was observed in response to the SASP. Interestingly, PLVAP inhibition resulted in a small but significant increase in lymphocyte transmigration from 37.3% to 44.1% (**Figure 5D**). Consistent with siRNA knockdown experiments, monocyte transmigration was selectively impaired following PLVAP antibody treatment, whilst there was also a slight reduction in monocyte adhesion that was not statistically significant (**Figure 5D**). These data suggest that PLVAP contributes to monocyte, but not lymphocyte, transmigration across

liver endothelium in response to the senescent cell secretome. To assess this in the setting of human disease *in situ*, we performed dual colour immunofluorescent staining of PLVAP alongside MAC387, as a marker of infiltrating monocytes, in samples of end-stage CLD. In support of a role for PLVAP in hepatic monocyte recruitment, we were able to spatially demonstrate that $MAC387^{+}$ cells were frequently found adhered to $PLVAP^{+}$ endothelium in CLD patient specimens (**Figure 5E**).

PLVAP regulates endothelial paracellular permeability by altering levels of phosphor-VE-cadherin and promoting endothelial gap formation.

Unlike CD31, PLVAP did not seem to be enriched around transmigrating monocytes, suggesting its role may be an indirect one (**Supplementary Figure 6A**). To elucidate the mechanisms by which PLVAP could regulate monocyte transmigration, bulk RNA sequencing was performed following RNA interference in LSEC. Following *PLVAP* knockdown, 50 genes were significantly downregulated and 79 genes were significantly upregulated compared to the negative control (*padj*<0.05) (**Figure 6A**). Gene ontology analysis revealed an enrichment of several pathways of interest, relating to the basement membrane, focal adhesions and adherens junctions (**Figure 6B, Supplementary Figure 6B**). We demonstrated a significant reduction of transendothelial electrical resistance (TEER), an inverse measurement of permeability, in response to SASP exposure which was reversed upon PLVAP knockdown (**Figure 6C**). These transcriptional and functional data support a significant role for PLVAP in regulating the barrier function of SASP stimulated LSEC. We hypothesised that PLVAP regulating junctional permeability which would explain the downstream effect on monocyte transmigration, given that these cells prefer to extravasate via the paracellular route (**Figure 4C**).

To test this hypothesis further, we focused on in the intercellular adherens junctions by using immunostaining for VE-cadherin (**Figure 6D**). Following SASP exposure, we noted the formation of spontaneous gaps in LSEC junctions without the presence of any transmigrating cells (**Figure 6D**), a phenomenon that has been described previously in endothelial cells(45). We found that frequency of these junctional gaps per cell was significantly reduced following PLVAP inhibition, suggesting these cells may have tighter adherens junctions in the presence of SASP. VE-cadherin is known to undergo phosphorylation in response to permeability-inducing stimuli such as VEGF, which leads to its internalisation from the junction. Immunostaining for phospho-VE-cadherin (Y658) indicated a similar pattern, whereby SASP treatment increased VE-cadherin phosphorylation. In parallel to the reduction in junctional gap formation, we found that SASP-driven phosphor-VE-cadherin upregulation was reversed in the setting of *PLVAP* knockdown (**Figure 6E**). Therefore, PLVAP has a significant role in regulating LSEC junctional integrity and mediating monocyte transmigration in response to the senescence secretome.

Discussion

The incidence of CLD continues to increase globally, and for end-stage liver disease and HCC patients, the overall survival remains extremely poor. The outcome of chronic liver injury and/or tumourigenesis is determined, at least in part, by the hepatic immune microenvironment. During chronic inflammation, sinusoidal endothelial cells undergo phenotypic changes that facilitate activation and leukocyte recruitment, which is almost certainly mediated by factors within the biological milieu[6]. Recent single-cell RNA sequencing studies have highlighted the re-emergence of PLVAP, a marker of foetal liver endothelium largely absent from the adult liver sinusoids, in human liver cirrhosis and HCC[15, 16]. Here, we validate PLVAP as a marker of scar-associated endothelium within neovessels and peri-fibrotic sinusoidal channels, demonstrating its upregulation in CLD and HCC. Although several soluble mediators of PLVAP expression have been identified in various endothelial cell types, including VEGF[31-34, 46], HGF[33], PMA[33, 35, 47], TNFα[12, 48], transforming growth factor β[48], BMP-9[49], angiotensin II[32] and fibrinogen[50], its specific regulation in primary human liver endothelia has not been studied previously. Given that hepatic endothelial cells are known to differ drastically from conventional endothelia in their transcriptional and metabolic profiles, expression of atypical adhesion molecules, and junctional characteristics[51], we sought to investigate PLVAP regulation in primary human LSEC. We found that PLVAP is regulated by several soluble mediators, notably the pro-angiogenic mediator VEGF, as well as conditioned medium from hepatocyte cell lines. Importantly, we also demonstrate a direct link between PLVAP expression and the senescent secretome, to our knowledge a new finding which could make a significant contribution to the upregulation of PLVAP under pathological conditions.

Cellular senescence, a state of proliferative arrest in which cells remain metabolically active, is a key feature of both CLD and HCC[17, 52]. Yet, the effects of senescence appear to be pleiotropic and are largely cell type- and context-dependent. For instance, senescence is thought to be a physiological response to cellular stress or damage which has evolved as a protective mechanism against malignant transformation. However, release of a distinct secretome (SASP) can be both beneficial and deleterious, driving pro- and anti-inflammatory responses[18]. The senescent cell secretome, a concoction of cytokines, chemokines and growth factors, has been shown to reinforce senescence in an autocrine and paracrine manner ("bystander effect"), aiming to alert and sensitise neighbouring cells to the stressful stimulus[53, 54]. Furthermore, the SASP activates immune responses to promote senescence surveillance. This surveillance is key in preventing senescent cell accumulation that can simultaneously drive chronic inflammation and foster a pro-tumourigenic niche[18, 19]. Our results provide evidence for a previously unreported relationship between PLVAP and senescence in CLD, whereby senescent cells are spatially enriched in close association with PLVAP$^+$ endothelium in patient specimens.

Endothelia within and proximal to fibrotic regions are known to be major sites for leukocyte recruitment[55] and we demonstrate here that peri-fibrotic PLVAP-rich areas were characterised by

infiltration of monocytes and lymphocytes. Moreover, we have previously reported that exposure of liver endothelial cells to the senescent cell secretome *in vitro* can drive recruitment of lymphocytes under physiologically low shear stress[21]. In this study, we demonstrate, using flow adhesion assays and primary human cells, that endothelial SASP-stimulation also facilitates the recruitment of monocytes. Furthermore, we provide evidence that SASP-mediated monocyte and lymphocyte recruitment differ on a molecular level, involving distinct transmigratory routes and adhesion molecules. Monocytes are known to transmigrate predominantly via the paracellular route in response to TNFα stimulation of HUVEC[56] and we confirm that this is also the case for SASP-treated LSEC. Similarly, our data suggest ~60% lymphocytes transmigrate transcellularly, which is consistent with our previous studies using TNFα/IFNγ-stimulated liver endothelia[44]. We utilised antibodies targeted against known adhesion molecules to characterise the mechanisms of SASP-mediated leukocyte recruitment. These studies highlighted an important role for CD31 in monocyte transmigration whilst ICAM1 was implicated in both lymphocyte adhesion and transmigration. Our findings are consistent with previous studies using LSEC and HUVEC, which report the formation of ICAM1-/F-actin-rich adhesive cups and transmigratory channels[44, 57], and CD31-/F-actin-rich membrane protrusions[58], associated with extravasating lymphocytes and monocytes, respectively.

Amongst its well-characterised functions in development, vascular permeability and angiogenesis, PLVAP has also been implicated in leukocyte trafficking both *in vitro* and *in vivo*. In the lymphatic system, PLVAP mediates lymphocyte and antigen entry into the lymph nodes by forming a size-selective sieve[13], whilst in the developing liver PLVAP regulates the egress of foetal liver monocytes and subsequent seeding as tissue-resident macrophages[14]. Yet, a role for PLVAP in adult hepatic leukocyte recruitment has not been studied previously. It has become clear that atypical adhesion molecules, including scavenger receptors, that are enriched in liver endothelia can recruit specific immune cell subsets. Such receptors include stabilin-1 (T_{reg} transmigration) and SCARF1 ($CD4^+$ T_{eff} adhesion)[44, 57]. We hypothesised that the disease-specific upregulation of PLVAP within the senescent hepatic microenvironment may be important for leukocyte recruitment. To investigate this, we performed flow adhesion assays with monocytes and lymphocytes following genetic knockdown or antibody-mediated blockade of PLVAP in SASP-treated LSEC. Our data indicate that PLVAP mediates monocyte, but not lymphocyte, transmigration in response to the senescent secretome.

We subsequently explored mechanisms by which PLVAP mediated monocyte transmigration by studying the transcriptional differences between LSEC in the presence and absence of PLVAP knockdown. The gene pathway analysis of our results suggested that PLVAP played a significant role in mediating LSEC barrier function and integrity by regulating the key pathways of focal adhesions, cell-cell and adherens junctions. We therefore studied the contribution of PLVAP to the barrier function in SASP-treated LSEC and how this could be impacting on monocyte transmigration. Firstly, we found that the SASP treatment did increase endothelial permeability with a TEER assay and that this could be rescued by PLVAP knockdown. Subsequently, we linked PLVAP- mediated

permeability to junctional changes that would promote paracellular migration by confirming alterations in VE-cadherin gap formation by promoting a shift towards increased Phospho-VE-cadherin expression.

LSEC phenotypic changes in human CLD are characterised by loss of fenestrae and the deposition of a basement membrane[59]. In parallel there is a re-emergence of the receptor PLVAP, previously shown to be expressed in fetal liver endothelium. Our data provides new insights on how the mechanistic switch in LSEC permeability during the transition from homeostasis to pathology can have an impact on immune cell diapedesis. Considering our data, we propose a mechanism in human CLD in which senescent cell-endothelial crosstalk drives expression of PLVAP and regulates junctional permeability in LSEC to facilitate monocyte recruitment (**Figure 7**). In the context of cellular senescence, our data provide new insights into the non-cell autonomous impact of the SASP on human liver endothelium. We provide evidence that innate and adaptive immune cell recruitment across liver endothelium occurs by distinct routes, following SASP stimulation, identifying PLVAP as a selective mediator of monocyte transmigration. There is strong evidence that senescence shapes the immune landscape in liver disease, as well as a range of other pathologies, and is an important therapeutic target for chronic inflammation and cancer risk. Despite this, successfully targeting cellular senescence to prevent its deleterious effects whilst maintaining its beneficial effects remains an unmet clinical need. Our study suggests that directly targeting liver endothelium, specifically PLVAP, could selectively shape the senescence-driven immune microenvironment and have a critical impact on tissue regeneration/cancer risk that accompanies chronic liver inflammation.

Limitations of the study

There are limitations to our study that need to be taken into account when interpreting the results. Primarily that the functional contribution of PLVAP to monocyte recruitment across liver endothelium has been demonstrated in an *in vitro* setting. We and others have confirmed that PLVAP is upregulated on liver endothelium in cirrhosis[15] and our functional analysis was performed on primary human liver endothelial cells. Additionally, we have used phase contrast microscopy and confocal imaging to study transmigration and the route of paracellular and transcellular migration across an endothelial monolayer. Nevertheless, the *in vitro* setting provides limitations with regard to a lack of a multicellular environment e.g. absence of pericytes and future *in vivo* studies with intravital microscopy would provide additional support for our work. The links with PLVAP upregulation associated with monocyte recruitment in liver tissue is correlative, future chronic liver injury models that are known to promote senescence could be undertaken in animal models in the setting of PLVAP knockout or inhibition, followed by analysis of monocyte infiltration by imaging and quantification. It is well established that macrophages are highly plastic and they have diverse roles in liver disease ranging from pathogen recognition to wound healing[60]. Our studies have focused on

the migratory impact of PLVAP on monocyte recruitment, the flow assay recapitulates recruitment within the hepatic sinusoidal channels but we are unable to retrieve transmigrated monocytes. Further *in vitro/in vivo* studies are required to assess if PLVAP has an additional impact on the polarisation and phenotype of transmigrated monocytes.

Author Contributions:

SS, MS, PR, MH: Conceptualisation, manuscript editing, supervision
ALW, DAP: Data generation/curation, methodology, writing, manuscript editing and revision
SH, JK, EM, PH, KY, MYWZ, GH, WL: Data generation
ELS: Resources, methodology
DHA: manuscript editing

Acknowledgements:

ALW was funded by a Wellcome Trust Ph.D studentship in Mechanisms of Inflammatory Disease and a follow-on fund awarded by the University of Birmingham. DAP and SS are funded by a Medical Research Council Project Grant (MR/R010013/1) and a Cancer Research UK Advanced Clinician Scientist Fellowship (C53575/A29959) awarded to SS. JIK is funded by an Engineering and Physical Sciences Research Council LifETIME CDT Ph.D studentship. MYWZ and SS are funded by the Newton Prize 2020 as a part of the UK's Official Development Assistance "ODA" and the Newton fund. MH is supported by a CRUK Advanced Clinician Scientist Fellowship (C52489/A19924); CRUK-OHSU Project Award (C52489/A29681) and CRUK Accelerator Award to the HUNTER consortium (C18873/A26813) funded through a partnership between Cancer Research United Kingdom, Fondazione AIRC and Fundación Científica de la Asociación Española Contra el Cáncer. This paper represents independent research supported by the NIHR Birmingham Biomedical Research Centre at the University Hospitals Birmingham NHS Trust and the University of Birmingham. The views expressed are those of the authors and not necessarily those of the NHS, the NIHR or the Department of Health and Social Care.

We thank the patients and clinical staff from the Queen Elizabeth Hospital, Birmingham, for donation and collection of tissue and blood. We also thank Dr Gary Reynolds, Subin Modit and Janine Fear for their technical assistance.

Declaration of Interest:

SS is a consultant for Faron Pharmaceuticals.

Inclusion and Diversity:

We support inclusive, diverse, and equitable conduct of research.

Figure 1: Plasmalemma vesicle-associated protein (PLVAP) is upregulated in chronic liver disease (CLD) and displays a scar-associated expression pattern.

(A) *PLVAP* gene expression in normal liver (NL) (n=6) vs. cirrhotic liver (n=24) was measured relative to *18S* by qRT-PCR. Data shown are median ± IQR (***p<0.001, Mann-Whitney test)

(B) Quantification of PLVAP immunohistochemical (IHC) staining (% area) in NL (n=6) and CLD (n=14) tissue (mean ± SEM, ***p<0.001 student's unpaired *t*-test). Isotype-matched control (IMC) level is indicated by the grey gridline

(C) Correlation between PLVAP and Sirius Red staining (% area) in matched patient samples (****p<0.0001, Pearson's correlation test)

(D) Representative IHC images of PLVAP and Sirius Red in matched serial sections from normal *(upper)* and cirrhotic *(lower)* human liver. Fibrotic septa are indicated by red dashed lines

(E) Dual immunofluorescent staining of PLVAP (red) with CD31 (*left*), L-SIGN (*middle*) and LYVE-1 (*right*) (green) in cirrhotic liver. DAPI (blue) was used as a nuclear counterstain. Yellow lines depict site of the intensity profiles (*lower*)

Figure 2: Plasmalemma vesicle-associated protein (PLVAP) correlates with senescence and immune infiltrate in chronic liver disease (CLD).

(A) Representative low (*upper*) and high (inset, *lower*) power images of immunohistochemical staining of PLVAP, Sirius Red and senescence markers, p21 and p16, in serial sections from matched CLD patient samples

(B) Correlation analysis of *PLVAP* vs. p21 (*CDKN1A*) (*left*) and *PLVAP* vs. p16 (*CDKN2A*) *(right*) mRNA levels in normal liver (NL) (n=5) and CLD (n=15). Gene expression was measured relative to *18S* by qPCR (*p<0.05, **p<0.01, Spearman's correlation test)

(C) Correlation analysis of PLVAP vs. p21 (*left*) (n=27) and PLVAP vs. p16 (*right*) (n=24) immunohistochemical staining in normal liver (NL) and CLD (*p<0.05, ***p<0.001, Spearman's correlation test)

(D) Representative immunohistochemical staining of PLVAP, MAC387 (infiltrating monocytes), CD3 (T cells) and CD20 (B cells) (*from left to right*) in serial sections from cirrhotic liver patient samples. Visual fields are the same for each marker

(E) Correlation analysis of PLVAP staining area (%) with MAC387, CD3 and CD20 (*from left to right*) in normal liver (NL) (n=3) and CLD (n=11-12) (*p<0.05, Spearman's correlation test)

Figure 3: Plasmalemma vesicle-associated protein (PLVAP) is maintained *in vitro* in primary liver sinusoidal endothelial cells (LSEC) and is upregulated by the senescent secretome.

(A) *PLVAP* gene expression in passaged LSEC, activated liver myofibroblasts (aLMF), hepatic stellate cells (HSC) and biliary epithelial cells (BEC) relative to *GAPDH* (n=5). Data shown

are mean ± SEM (****p<0.0001, one-way ANOVA followed by Holm-Šídák's multiple comparisons test)

(B) Confocal images of PLVAP (red) immunofluorescence (white arrowheads) in patient-derived LSEC (25x objective) (*left*) and with junctional marker, VE-cadherin (green) (*right*) (63x objective). DAPI (blue) was used as a nuclear counterstain

(C) *PLVAP* gene expression relative to *GAPDH* in LSEC following 24 h treatment with the senescent secretome (Ras-CM) or the growing control (Grow-CM) (*p<0.05, Wilcoxon test) (n=7)

(D) PLVAP immunofluorescence area *(left)* and intensity *(right)* following Grow-CM or Ras-CM treatment. Staining was quantified via high-content imaging where nine visual fields per well were analysed with each condition performed in at least duplicate. Data shown are mean ± SEM from four independent cell isolates (*p<0.05, student's unpaired *t*-test (area) or Mann-Whitney test (intensity). Isotype-matched control (IMC) levels are indicated by the grey gridline

(E) Representative immunofluorescent images of PLVAP (green) in LSEC following 24 h Grow-CM or Ras-CM treatment. DAPI (blue) was used as a nuclear counterstain

Figure 4: The senescent secretome drives recruitment of lymphocytes and monocytes across primary human liver sinusoidal endothelial cells (LSEC) by distinct molecular mechanisms

(A) Flow adhesion assays were performed with peripheral blood monocytes and primary LSEC following Grow-CM or Ras-CM stimulation for 24 hours. Representative phase-contrast images are shown indicating adhered (yellow arrowheads), shape-changed (red arrowheads) and transmigrated (black arrowheads) monocytes

(B) Quantification of adhered, shape-changed and transmigrated monocytes following flow assays with Grow-CM- or Ras-CM-treated LSEC. Data shown are mean ± SEM from six independent experiments where ten visual fields were analysed per condition (*p<0.05, **p<0.01, ***p<0.001, Mann-Whitney test (adhered and % transmigrated) or student's unpaired *t*-test)

(C) Confocal images of LSEC pre-labelled with CellTracker Green (green) and SiR-actin (red) following flow assays with monocytes (*upper*) or lymphocytes (*lower*). Paracellular (yellow arrowheads) and transcellular (yellow arrows) transmigration (TM) was determined based on integrity of VE-cadherin$^+$ intercellular junctions (grey). Quantification of transmigratory route as a percentage of total TM events is shown (159 lymphocyte events and 327 monocyte events). Data are mean ± SEM from three independent cell isolates

(D) Quantification of adhered and transmigrated (% adhered) monocytes (*left*) and lymphocytes (*right*) following antibody-mediated blockade of intercellular adhesion molecule 1 (ICAM-1) (*p<0.05, Mann-Whitney test)

(E) Quantification of adhered and transmigrated (% adhered) monocytes (*left*) and lymphocytes (*right*) following antibody-mediated blockade of CD31 (**p<0.01, student's unpaired t-test)

(F) Orthogonal confocal images of monocyte (*upper*) and lymphocyte (*lower*) TM. LSEC were pre-labelled with CTG (green) and SiR-actin (grey). CD31 (*upper*) and ICAM-1 (*lower*) were stained post-fixation (red)

(G) 3-D rendered images of z-stacks showing monocyte (*upper*) and lymphocyte (*lower*) TM in association with CD31 and ICAM-1, respectively (red)

Figure 5: Plasmalemma vesicle-associated protein (PLVAP) mediates monocyte, but not lymphocyte, transmigration across patient-derived liver sinusoidal endothelial cells (LSEC) in response to the senescent secretome.

(A) Genetic knockdown of PLVAP was performed via siRNA transfection of LSEC and efficiency was validated at the mRNA and protein level by qRT-PCR and immunofluorescence, respectively (**p<0.01, ****p<0.0001, student's unpaired t-test)

(B) Flow adhesion assays were performed following PLVAP knockdown (siPLVAP) with Ras-CM-treated LSEC and either monocytes or lymphocytes. Representative phase-contrast images of monocytes are shown. Adhered and transmigrated (% adhered) monocytes and lymphocytes were quantified in ten visual fields per lane with each condition performed in duplicate. Data shown are mean ± SEM from 3-4 independent experiments (***p<0.001, student's unpaired t-test)

(C) Quantification of antibody binding (% area) following treatment of live LSEC with an anti-PLVAP antibody or isotype-matched control (IMC). Cells were then fixed, permeabilised and stained with an anti-mouse AlexaFluor 488 secondary antibody. Representative images are shown. Data are mean ± SEM from three independent experiments (*p<0.05, student's unpaired t-test)

(D) Flow adhesion assays were performed following antibody-mediated PLVAP blockade with Ras-CM-treated LSEC and either monocytes or lymphocytes. Representative phase-contrast images of monocytes are shown. Adhered and transmigrated (% adhered) monocytes and lymphocytes were quantified in ten visual fields per lane with each condition performed in duplicate. Data shown are mean ± SEM from three independent experiments (*p<0.05, student's unpaired t-test)

(E) Dual immunofluorescent staining of PLVAP (green) and MAC387 (red) in human liver cirrhosis. DAPI (blue) was used as a nuclear counterstain

Figure 6: Plasmalemma vesicle-associated protein (PLVAP) regulates endothelial paracellular permeability by altering intercellular junctions.

(A) Genetic knockdown of *PLVAP* was performed via siRNA transfection of LSEC (n=3) and RNA was extracted and subject to bulk RNA sequencing. Heatmap indicates significant differential gene expression and specific genes from gene ontology pathway analysis are highlighted

(B) Gene ontology (GO) cellular component pathway analysis. Unfilled bars indicate downregulation and filled bars indicate upregulation in siPLVAP cells. Relevant pathways are highlighted in green

(C) Transendothelial electrical resistance (TEER) of LSEC monolayers following *PLVAP* knockdown (siPLVAP) or negative control (siControl) in the presence (Ras-CM) or absence (Grow-CM) of the senescent secretome. Data shown are mean fold-change to control ± SEM from three independent LSEC isolates (**p*<0.05, paired *t*-test)

(D) Confocal images of VE-cadherin (red) in LSEC following *PLVAP* knockdown and 24 h Ras-CM treatment. DAPI (blue) was used as a nuclear counterstain. Junctional gaps *(lower)* were scored manually for six visual fields per condition and normalised to the cell count. Data shown are mean ± SEM from three independent LSEC isolates (**p*<0.05, *****p*<0.0001, one-way ANOVA and Tukey's post-hoc test)

(E) Confocal images of phospho-VE-cadherin (Y658) (green) in LSEC following *PLVAP* knockdown and 24 h Ras-CM treatment. DAPI (blue) was used as a nuclear counterstain. pVE-cadherin % staining area *(lower)* was quantified for six visual fields per condition. Isotype-matched control (IMC) level is indicated by the grey gridline. Data shown are mean ± SEM from three independent LSEC isolates (***p*<0.01, ****p*<0.001, one-way ANOVA and Tukey's post-hoc test)

STAR METHODS

Key Resources Table

REAGENT or RESOURCE	SOURCE	IDENTIFIER
Antibodies		
PLVAP	Novus Biologicals	Cat# NBP1-83911; RRID:AB_11029033
Anti-rabbit IgG HRP	Sigma	Cat# A0545; RRID:AB_257896
β-actin	Sigma	Cat# A5441; RRID:AB_476744
Anti-Mouse IgG HRP	Sigma	Cat# A4416; RRID:AB_258167
PLVAP	Abcam	Cat# ab8086; RRID:AB_306255
MR	Abcam	Cat# ab64693; RRID:AB_1523910
L-SIGN	R&D	Cat# MAB162; RRID:AB_2244985
LYVE-1	R&D	Cat# MAB20891; RRID:AB_2297198
CD31	Dako	Cat# M0823; RRID:AB_2114471

CD34	Abcam	Cat# ab8536; RRID:AB_306607
Vimentin	Sigma	Cat# V6389; RRID:AB_609914
PLVAP	Sigma	Cat# HPA002279; RRID:AB_1079636
p21	Dako	Cat# M7202; RRID:AB_2077700
p16	Abcam	Cat# ab54210; RRID:AB_1608104
MAC387	Invitrogen	Cat# MA5-12213; RRID:AB_10981946
CD3	Dako	Cat# M7254; RRID:AB_2631163
CD20	Invitrogen	Cat# MA5-13141; RRID:AB_10983209
NE	Abcam	Cat# ab219585; RRID:AB_11155265
PLVAP	Abcam	Cat# ab81719; RRID:AB_1658370
VE-cadherin	R&D	Cat# MAB9381; RRID:AB_2260374
ICAM-1	R&D	Cat# BBA3; RRID:AB_356950
CCL2	Novus Biologicals	Cat# NBP1-07035; RRID:AB_1625612
GM130	BD Biosciences	Cat# 610823; RRID:AB_398142
CD31	Abcam	Cat# ab9498; RRID:AB_307284
Anti-Mouse Immpress® Kit	Vector	Cat# MP-7402; RRID:AB_2336528
Anti-Rabbit Immpress® Kit	Vector	Cat# MP-7401; RRID:AB_2336529
Anti-mouse IgG1 AF488	Invitrogen™	Cat# A21121; RRID:AB_2535764
Anti-mouse IgG1 AF546	Invitrogen™	Cat# A21123; RRID:AB_2535765
Anti-mouse IgG2a AF546	Invitrogen™	Cat# A21133; RRID:AB_2535772
Anti-mouse mIgG2b AF488	Invitrogen™	Cat# A21141; RRID:AB_2535778
Anti-mouse IgG2b AF546	Invitrogen™	Cat# A21143; RRID:AB_2535779
Anti-rabbit AF488	Invitrogen™	Cat# A11008; RRID:AB_143165
Anti-rabbit AF546	Invitrogen™	Cat# A11035; RRID:AB_2534093
Anti-EpCAM antibody (clone HEA125)	Progen	Cat# 61004 RRID:AB_2920684
Biological samples		
Explanted human liver tissues	Queen Elizabeth Hospital, Birmingham, UK.	LREC Approval 06/Q2702/61, 18/WA/0214 and 18/LO/0102, South Birmingham, Birmingham, UK.

Healthy volunteer blood	University of Birmingham, Birmingham, UK	LREC Approval 18/WA/0214, South Birmingham, Birmingham, UK.
Chemicals, peptides, and recombinant proteins		
Percoll™	Sigma	Cat# GE17-0891-01
Endothlelial Cell Serum-Free Medium	Gibco	Cat# 11111044
HGF	Peprotech	Cat# 100-39H
VEGF	Peprotech	Cat# 100-21
Collagen type I from rat tail	Sigma	Cat# C3867
Lympholyte® Cell Separation Media	Cedarlane	Cat# CL5020
SiR-actin Live Cell Actin Probe	Spirochrome	Cat# SC001
CellTracker™ Green (CMFDA)	Invitrogen	Cat# C2925
TNFα	Peprotech	Cat# 300-01A
RNAi Max Lipofectamine	Invitrogen	Cat# 13778-075
Direct red 80	Sigma	Cat# 365548
ImmPACT® DAB Peroxidase (HRP) Substrate	Vector	Cat# SK-4105
Picric acid (1.3% v/v)	Sigma	Cat# P6744-1GA
SuperScript® III Reverse Transcriptase	Invitrogen	Cat# 18080-044
TaqMan® Universal PCR Master Mix	Applied Biosystems	Cat# 4326708
SuperScript® III Reverse Transcriptase	Invitrogen	Cat# 18080-044
TaqMan® Universal PCR Master Mix	Applied Biosystems	Cat# 4326708
Phalloidin AF633	Invitrogen	Cat# A22284
Critical commercial assays		
Pan Monocyte Isolation Kit (Human)	Miltenyi Biotec	Cat# 130-096-537
RNeasy® Micro Kit	Qiagen	Cat# 74004
RNeasy® Mini Kit	Qiagen	Cat# 74104
Dynabeads™ CD31 Endothelial Cell	ThermoFisher Scientific	Cat# 11155D
Dynabeads™ Goat Anti-Mouse IgG	ThermoFisher Scientific	Cat# 11033
Dynabeads™ CD45	ThermoFisher Scientific	Cat# 11153D
Ibidi® ibiTreat µ-Slide VI 0.4	Ibidi	Cat# 80606
Deposited data		
PLVAP siRNA knockdown in human LSEC	Gene Expression Omnibus; https://www.ncbi.nlm.nih.gov/geo/	GEO: GSE222993
Experimental models: Cell lines		
HepG2	ATCC	Cat# HB-8065; RRID:CVCL_0027
IMR90	ATCC	Cat# CCL-186; RRID:CVCL_0347
Oligonucleotides		

Negative Control siRNA	Ambion	Cat# 4390843
PLVAP siRNA	Ambion	Cat# s37972
18S TaqMan® Assay	ThermoFisher Scientific	Cat# Hs99999901
ACTB TaqMan® Assay	ThermoFisher Scientific	Cat# Hs01060665
CCL2 TaqMan® Assay	ThermoFisher Scientific	Cat# Hs00234140
CDKN1A TaqMan® Assay	ThermoFisher Scientific	Cat# Hs00355782
CDKN2A TaqMan® Assay	ThermoFisher Scientific	Cat# Hs00923894
CXCL8 TaqMan® Assay	ThermoFisher Scientific	Cat# Hs00174103
GAPDH TaqMan® Assay	ThermoFisher Scientific	Cat# Hs99999905
GUSB TaqMan® Assay	ThermoFisher Scientific	Cat# Hs00939627
ICAM1 TaqMan® Assay	ThermoFisher Scientific	Cat# Hs00164932
IL1B TaqMan® Assay	ThermoFisher Scientific	Cat# Hs00174097
IL6 TaqMan® Assay	ThermoFisher Scientific	Cat# Hs00985639
PLVAP TaqMan® Assay	ThermoFisher Scientific	Cat# Hs00229941

Resource Availability

Lead contact

Further information and requests for resources and reagents should be directed to and will be fulfilled by the lead contact, Prof. Shishir Shetty (s.shetty@bham.ac.uk).

Materials availability

This study did not generate any new unique reagents.

Data and code availability

RNA-sequencing data has been deposited on GEO repository and are publicly available under the accession number GSE222993.
This paper does not report any original code.
Any additional information required to reanalyse the data reported in this paper is available from the lead contact upon request.

Experimental Model and Study Participant Details

Human tissue and blood

All human tissue was obtained with prior written informed consent and ethically approved for use in research. Explant human liver tissue was collected from patients undergoing liver transplantation at the Queen Elizabeth Hospital Birmingham under ethical study numbers 06/Q2702/61, 18/WA/0214 and 18/LO/0102. Normal liver tissue was obtained from rejected organ donors deemed unsuitable for transplantation under ethical study numbers 06/Q2702/61 and 18/WA/0214. Patient gender/age are provided in Supplementary Tables 1 and 2. Peripheral blood samples were taken from healthy volunteers under ethical study number 18/WA/0214.

Cell lines

HepG2 cells (ATCC) and IMR90 cells (ATCC) were cultured in Dulbecco's modification of Eagle's medium (DMEM; GIBCO), supplemented with 10% fetal bovine serum, 100 units/ml penicillin, 100 µg/ml streptomycin and 1% L-glutamine. Cells were maintained in a humidified incubator at 37°C and with 5% CO_2.

Method Details

Quantitative real-time (qRT)-PCR

RNA was isolated from whole liver tissue or cell lysates using the RNeasy® Mini Kit (Qiagen) or RNeasy® Micro Kit (Qiagen), respectively, as per the manufacturer's instructions. These kits were used in conjunction with the RNase-Free DNase Set (Qiagen). Approximately 20-30 mg of liver tissue was homogenised in gentleMACS™ M-tubes (Miltenyi Biotec) containing RLT buffer (RNeasy® Kit) using a gentleMACS™ Dissociator (Miltenyi Biotec). Alternatively, primary liver cells were cultured in 6-well TC-treated plates (Corning®) and lysed *in situ* with RLT buffer containing 1% β-mercaptoethanol. Following RNA extraction, quantity and purity were assessed using a NanoPhotometer™ (Geneflow), and reverse transcription was performed using the SuperScript® III Reverse Transcriptase Kit (ThermoFisher Scientific). qRT-PCR was performed in triplicate to assess mRNA expression using TaqMan® Gene Expression Assays (Applied Biosystems®) and TaqMan® Universal PCR Master Mix. Reactions were performed in a LightCycler® 480 (Roche) by completing 40 cycles of the following programme: 95°C for 10 seconds; 60°C for 50 seconds; 72°C for one second. Gene expression was normalised to an appropriate housekeeping gene (*GAPDH* for cells, *18S* for CLD tissue, *GUSB* for HCC tissue) using "E-analysis" software (Roche).

Western blot

Approximately 75 mg of frozen liver tissues were homogenised in gentleMACS™ M-tubes (Miltenyi Biotec) containing CelLytic™ MT lysis buffer (Sigma), 0.1% Protease Inhibitor Cocktail (Sigma), 1%

Phosphatase Inhibitor Cocktail 3 (Sigma) and 5 U/mL DNase-I (Sigma). Protein concentration was determined by bicinchoninic acid (BCA) assay (Sigma), using bovine serum albumin (BSA) as a protein standard, and subsequently diluted to a concentration of 2 mg/mL in CelLytic™ MT lysis buffer before storage at -20°C. Protein lysates (20 µg) were separated on a 10% SDS-PAGE and transferred to nitrocellulose membranes (ThermoFisher Scientific) before blocking with 5% non-fat milk solution (Marvel) in PBS + 0.02% Tween20 (Sigma) (PBS/T) for one hour at 20-22°C. Primary antibody was incubated overnight at 4°C before washing three times with PBS/T followed by addition of a horseradish peroxidase (HRP)-conjugated anti-rabbit IgG antibody and incubation for one hour at 20-22°C. Following three additional wash steps with PBS/T, protein bands were detected using Pierce™ Enhanced Chemiluminescence (ECL) Substrate (ThermoFisher Scientific). Membranes were stripped with Restore™ Western Stripping Buffer (ThermoFisher Scientific) for ten minutes before repeating blocking and incubation steps above to probe for β-actin. After washing, membranes were incubated with HRP-conjugated anti-mouse IgG antibody for one hour. Protein bands were detected as described above.

Immunohistochemical, immunofluorescent and histological tissue staining

Immunohistochemistry was performed on 7 µm-thick acetone-fixed cryo-sections and 3 µm-thick formalin-fixed paraffin-embedded (FFPE) sections. Frozen sections were thawed to 20-22°C and hydrated with PBS/T (0.1%) for five minutes. FFPE sections were de-waxed and rehydrated by static sequential incubation for three minutes in xylene (3x), industrial denatured alcohol (3x), and water (2x). Heat-induced epitope retrieval was performed for FFPE sections for 20-30 minutes using 1% Tris-based (pH 9) or Citrate-based (pH 6) Antigen Retrieval Buffer (Vector Laboratories) followed by washing with TBS/T. Endogenous peroxidase activity was blocked using Bloxall® Endogenous Blocking Solution (Vector Laboratories) for 15 minutes, followed by one PBS/T or TBS/T wash. To block non-specific antibody binding, sections were incubated with 2X casein solution (Vector Laboratories) in PBS/TBS for 20 minutes at 20-22°C. For immunofluorescent (IF) staining of cryo-sections, blocking of non-specific binding was performed immediately after thawing and rehydration, with 2X casein containing 10% goat serum in PBS, for 20 minutes at 20-22°C.

Primary antibodies were incubated for one hour at 20-22°C, or overnight at 4°C (p21), before two five-minute PBS/T or TBS/T washes. Isotype-matched controls at equivalent concentrations were performed for each batch of staining. Sections were then incubated with an appropriate HRP-conjugated secondary antibody (Anti-Mouse [#MP-7402] or Anti-Rabbit [#MP-7401] Immpress® Kit, Vector Laboratories), or fluorescently-conjugated secondary antibody (Invitrogen), for 30 minutes at 20-22°C before two additional five-minute wash steps with PBS/T or TBS/T. Chromogenic staining was visualised by incubating with ImmPACT® DAB Peroxidase (HRP) Substrate (Vector Laboratories #SK-4105) for five minutes followed by PBS/T or TBS/T wash. For IF staining, DAPI

682 was used as a nuclear counterstain (300 nM in distilled water) by incubating with sections for five
683 minutes followed by washing with PBS/T or TBS/T. Autofluorescence of FFPE sections was
684 quenched using TrueView® Autofluorescence Quenching Kit (Vector Laboratories) as per the
685 manufacturer's instructions. Sections were then mounted using VECTASHIELD® Vibrance™
686 Antifade Mounting Medium (IHC-P) or ProLong™ Gold Antifade Mountant (IHC-Fr).

687 Sirius Red staining was performed on matched serial liver sections, where possible, by incubating
688 sections with 5% phorbol 12-myristate 13-acetate (PMA) in dH_2O for five minutes, followed by
689 incubation for 30-60 minutes with Sirius Red solution (1.3% picric acid containing 1 g/L Direct Red
690 80, Sigma). Sirius Red was then briefly replaced with 0.1 M hydrochloric acid before rinsing with
691 distilled water. For chromogenic and Sirius Red staining, Mayer's Haematoxylin (pfm Medical) was
692 used as a nuclear counterstain by incubating with sections for one minute before washing in warm
693 water for two minutes. Stained sections were then cleared and dehydrated in industrial denatured
694 alcohol (3x) and xylene (3x) before being mounted with DPX (Phthalate-free) mounting medium
695 (CellPath).

696 All stained sections were imaged using an Axio Scan.Z1 slide scanner and visual fields were
697 selected post-acquisition using ZEN blue software (Zeiss). To quantify immunohistochemical
698 staining, the "Threshold" and "Measure" functions of ImageJ software were used to give a mean %
699 positive staining area for five visual fields, allowing comparison of expression between liver samples.

700

701 *Primary cell isolation and culture*

702 All cells were cultured at 37°C in a humidified incubator with 5% CO_2 in tissue culture flasks
703 (Corning®). Following isolation, all cells were passaged using TrypLE™ Express Enzyme (1X)
704 (Gibco). Primary LSEC, activated liver myofibroblasts (aLMF), quiescent hepatic stellate cells (HSC)
705 and biliary epithelial cells (BEC) were isolated from ~30 g slices of explanted human liver as
706 previously described(30, 61, 62). Briefly, tissue was mechanically and enzymatically digested (10
707 mg/mL collagenase in PBS, Sigma), before separation of the non-parenchymal cell fraction by
708 centrifugation (800 *g* for 20 minutes) on a 33%:77% Percoll (GE Healthcare) density gradient.
709 Immune cells were depleted by positive immunomagnetic selection using CD45-conjugated
710 Dynabeads™ (Invitrogen). BEC were isolated by positive immunomagnetic selection for epithelial
711 cell adhesion molecule (EpCAM, Progen #61004, 4.55 µg/mL) using Goat Anti-Mouse IgG
712 Dynabeads™ (Invitrogen). BEC were maintained in Ham's F12 Medium and DMEM (1:1)
713 supplemented with 10% human serum (TCS Biosciences), 1% penicillin-streptomycin-glutamine
714 (PSG) (Gibco), 10 ng/mL epidermal growth factor (EGF, Peprotech), 10 ng/mL hepatocyte growth
715 factor (HGF, Peprotech), 0.124 IU/mL insulin, 2 µg/mL hydrocortisone, 10 ng/mL cholera toxin
716 (Sigma) and 2 nM tri-ido-thyronine (Sigma). Endothelial cells were isolated by positive
717 immunomagnetic selection using CD31 antibody-conjugated Dynabeads™ (Invitrogen) and seeded

in rat tail collagen (RTC)-coated (40 µg/mL) tissue culture flasks. LSEC were maintained in Human Endothelial Serum-free Medium (Gibco) supplemented with 10% human serum, 1% PSG, 10 ng/mL VEGF (Peprotech) and 10 ng/mL HGF. Whilst some phenotypic loss of LSEC *in vitro* will occur, we have previously demonstrated that the primary human LSEC isolated from diseased liver tissue using our technique still maintain their critical phenotypic features of scavenger receptor expression and highly efficient endocytosis and maintain a distinct gene signature compared to conventional endothelium, human umbilical vein endothelial cells, up to passage 5(51). Endothelial cells were used up to passage 5 except in flow assays where only passage 4 cells were used. Following removal of BEC and endothelial cells, remaining cells were considered to be a heterogenous population of aLMFs, which were cultured in Dulbecco's Modified Eagle Medium (DMEM) (Gibco) supplemented with 16% foetal bovine serum (FBS) (Gibco) and 1% PSG. Quiescent HSCs were isolated only from non-fibrotic liver tissue, cultured in DMEM containing 16% FBS and 1% PSG, and used up to passage 4.

Immunocytochemistry

Endothelial cells were seeded in RTC-coated ibiTreat µ-slide VI 0.4 (Ibidi®) and grown to confluence before being fixed with 4% paraformaldehyde for 10-15 minutes at 37°C. All remaining incubation steps were performed at 20-22°C with gentle agitation. Cells were permeabilised by incubating with 0.3% Triton X-100 in PBS for five minutes, before blocking with PBS containing 2X casein buffer and 10% goat serum for 20 minutes. Primary antibodies were then diluted in PBS and incubated for one hour followed by three PBS/T (0.1%) washes. Cells were incubated with fluorescently-conjugated secondary antibodies for 30 minutes before three additional wash steps. DAPI (300 nM in dH_2O) was used as a nuclear counterstain and incubated for five minutes before one PBS/T wash followed by addition of PBS. For relevant experiments, Phalloidin Alexa Fluor™ 633 (Invitrogen) was used to stain F-actin. Stained cells were stored at 4°C prior to imaging on a LSM880 confocal microscope (Zeiss).

High-content imaging

Primary human liver sinusoidal endothelial cells (LSEC) were seeded in RTC-coated black 96-well imaging plates (Falcon®) and grown to confluence. Cells were then serum- and growth factor-starved for two hours before 24-hour treatment with 10 ng/mL tumour necrosis factor α (TNFα), 100 ng/mL VEGF, conditioned medium from HepG2 hepatoma cells, or a relevant vehicle control. HepG2 cells were cultured in DMEM supplemented with 10% FBS and 1% PSG. Prior to harvesting of supernatants, HepG2 cells were grown to approximately 80% confluence, before passaging into two flasks and taking conditioned medium 24 hours after splitting. Supernatants were centrifuged at 300 *g* for five minutes to remove cell debris and stored at -20°C prior to use in high-content imaging

assays. Following treatment, LSEC were fixed with 4% PFA for 10-15 minutes and PLVAP was visualised by immunocytochemistry as described above. Images were acquired on a CellInsight™ CX5 High Content Screening Platform (ThermoFisher Scientific) and immunofluorescence was analysed using integrated HCS Studio™ Cell Analysis Software. A spot detection algorithm was applied to detect signal, on a per cell basis, within a defined region of interest relative to a primary object (cell nucleus). "Object.SpotTotalArea.Ch2" and "Object.SpotTotalInten.Ch2" were chosen as the most appropriate parameters to give fluorescence area and intensity measurements, respectively (**Supplementary Figure 2**).

SASP generation and stimulation

The SASP was generated by obtaining conditioned medium from IMR90 cells, expressing a 4-hydroxytamoxifen (4-OHT)-inducible form of oncogenic $HRAS^{G12V}$ (ER:$HRAS^{G12V}$), undergoing oncogene-induced senescence (21). ER:$HRAS^{G12V}$ IMR90 cells were generated using the pLNCX2 ER:ras (Addgene #67844; RRID:Addgene_67844) retroviral vector and maintained in DMEM supplemented with 10% FBS and cultured at 37°C in 5% CO_2. Cells were cultured in the presence or absence of 100 nM 4-OHT (Sigma) and conditioned medium was harvested on day 6, centrifuged at 300 *g* for five minutes, and stored at -80°C until use. The SASP was designated "Ras-CM" and the growing control was designated "Grow-CM". LSEC were treated with either Ras-CM or Grow-CM diluted in endothelial medium (1:1 or 1:3 ratio) for 24 hours before downstream analysis (i.e. qRT-PCR, immunocytochemistry, flow adhesion assays).

RNA interference

LSEC were seeded in RTC-coated 6-well or 96-well plates and analysis of knockdown efficiency at the mRNA and protein level was performed by qRT-PCR and high-content imaging, respectively. For use in flow adhesion assays, LSEC were seeded in RTC-coated ibidi® µ-slides and siRNA knockdown was performed *in situ.* siRNA duplexes (PLVAP, Ambion® #s37972; negative control, Ambion® #4390843) were diluted in Opti-MEM™ Reduced Serum Medium (Gibco), such that the final concentration was 3.125 nM, and incubated at 20-22°C for 10 minutes. RNAi Max Lipofectamine™ (Invitrogen) was diluted in Opti-MEM™ to a final concentration of 0.3% and incubated for 10 minutes at 20-22°C. Lipofectamine and siRNA solutions were then mixed and incubated for a further 10 minutes at 20-22°C, before addition of Opti-MEM™ to a final volume of 1 mL/well for 6-well plate and 200 µL/well for 96-well plates and ibidi® µ-slides. Cells were washed twice with PBS and then siRNA/lipofectamine solution was incubated with LSEC at 37°C for four hours. This was then replaced with antibiotic- and growth factor-free culture medium and incubated for 48 hours, prior to cell lysis, fixation, or use in flow adhesion assays.

Leukocyte Isolation

Peripheral blood mononuclear cells (PBMCs) were isolated from whole blood using Lympholyte® cell separation medium (Cedarlane) and centrifugation at 800 *g* for 20 minutes with no brake. To isolate lymphocytes, PBMCs were resuspended in flow assay medium (Endothelial SFM + 0.1% bovine serum albumin) and placed in a TC-treated culture flask for one hour to allow monocyte adhesion. Floating cell suspension was then harvested, centrifuged, and resuspended in flow assay medium at a cell density of 1 x 10^6/mL. Monocytes were isolated from the PBMC fraction by negative immunomagnetic selection using a Pan Monocyte Isolation Kit (Miltenyi Biotec) according to the manufacturer's instructions. Briefly, PBMCs were incubated for five minutes on ice with Fc Receptor Blocking Reagent and Biotin-Antibody Cocktail diluted in ice-cold magnetic-associated cell sorting (MACS) buffer (PBS + 1 mM ethylenediaminetetraacetic acid (EDTA) and 2% FBS). Then, Anti-Biotin Microbeads were added and further incubated on ice for ten minutes. Labelled cell suspension was then added to a pre-wetted LS column (Miltenyi Biotec) fitted within a Magnet Midi MACS (Miltenyi Biotec), followed by three MACS buffer washes (3 mL) and collection of the flow-through. Monocytes were kept in MACS buffer until required and then resuspended in flow assay medium at a cell density of 1 x 10^6/mL.

Flow adhesion assay

Flow adhesion assays were performed to recapitulate leukocyte recruitment within the hepatic sinusoids as previously described[42]. Approximately 75,000 LSEC per channel were seeded into RTC-coated ibidi® µ-slides and allowed to form an endothelial monolayer overnight. LSEC were stimulated for 24 hours prior to flow assay with either Grow-CM or Ras-CM diluted in Endothelial SFM (1:1 for lymphocytes, 1:3 for monocytes). All flow assay conditions were performed in duplicate. For siRNA knockdown experiments, flow assays were performed on day four (48 hours post-knockdown), whilst all other flow assays were performed on day three. For antibody-blockade experiments, LSEC were treated with 10 µg/mL relevant antibody or isotype-matched control (IMC) for 40 minutes, and flow assays were performed immediately thereafter. Leukocytes were perfused over LSEC at a physiological shear of 0.05 Pa for five minutes/channel, at a density of 1 x 10^6/mL, followed by a three-minute wash with flow assay medium. Phase-contrast recordings were taken against the flow direction. The use of a phase contrast microscope allows clear delineation of leukocytes adherent to the endothelial layer but remaining on the luminal side (phase bright in appearance) and those that have performed diapedesis and are below the endothelial layer (phase dark), as previously described[42]. Leukocyte adhesion, shape-change and transmigration were scored manually using ImageJ for ten visual fields/channel. Mean cell counts per channel were then normalised to cells/mm^2/10^6 cells perfused using the following equation:

$$N = \frac{c}{r \times b \times a \times l}$$

where N is the normalised count, c is the cell count per visual field, r is the flow rate (0.28 mL/min), b is the bolus time (5 min), a is the visual field area (0.154 mm^2) and l is the leukocyte density (1 x 10^6/mL)

The proportion of cells undergoing activation (shapechange) and transendothelial migration are expressed as a % of the total adherent cells.

Analysis of Leukocyte Rolling, Adhesion and Transmigration

Recorded fields of view were analysed offline and the number of adhered, shape-changed and transmigrated cells were scored manually by eye using the "Cell Counting" plugin on ImageJ. Stable, round, phase-bright leukocytes were counted as "adhered", whilst leukocytes that were phase-dark were considered "transmigrated". Shape-changed cells were no longer round and could be partially phase-bright/phase-dark.

To characterise the route of leukocyte transmigration in response to the senescent secretome, flow adhesion assays were performed with fluorescently-labelled (CellTracker Green and SiR-actin) Ras-CM-treated LSEC and peripheral blood monocytes or lymphocytes. Transmigration events were first identified by the presence of a leukocyte (visualised with DAPI and distinguished from LSEC nuclei based on size), along with disruption of the LSEC cytoplasm (CellTracker Green), which allowed differentiation between leukocytes adhered to the LSEC monolayer and those protruding through the LSEC cell body. Route of was transmigration was first determined by the location of diapedesis, ie. at the cellular junction or not, and then by the following: 1) transcellular transmigration was further identified by the presence of an actin-rich 'ring' around the leukocyte, visualised by pre-labelling the LSEC cytoskeleton with the live cell actin probe, SiR-actin. 2) paracellular transmigration was further identified by a definitive break in the integrity of VE-cadherin staining at the cell junctions.

Transendothelial electrical resistance (TEER) assay

Approximately 150,000 LSEC were seeded into RTC-coated 24-well Millicell transwell inserts (polyethylene terephthalate, 0.4 μm; EMD Millipore) and allowed to form an endothelial monolayer overnight. siRNA knockdown was performed *in situ* and LSEC were then incubated in antibiotic- and growth factor-free culture medium for 24 hours. LSEC were stimulated for a further 24 hours, prior to the TEER assay, with Ras-CM diluted in Endothelial SFM (1:3). All conditions were performed in duplicate. Transendothelial electrical resistance (TEER) was measured using a Millicell-ERS2 Volt-Ohm Meter (EMD Millipore) and expressed in Ωcm^2.

RNA sequencing

Paired end 2x150 bp RNA sequencing was performed by Source BioScience and we received raw sequencing files after adapter trimming. Transcript expression was quantified using the selective-alignment mapping algorithm implemented in *Salmon* (v1.5.2)[63] using a decoy-aware transcriptome index built from the reference genome GRCh38.p13 and the Gencode version 38 transcriptome. *Salmon* quantification was run with *--validateMappings*, *--gcBias* and *--seqBias* options and otherwise default settings. Gene-wise count summarisation and data import into R version 4.1.2 was performed with *tximport*[64]. Differential gene expression analysis was done using *DESeq2* (v1.34.0) with *independentFiltering* set to false and otherwise default settings[65]. Batch effects between LSEC samples from different livers were accounted for by including the liver sample identity into the design formula. Effect sizes were adjusted by Bayesian shrinkage of $\log_2$-fold changes as implemented in the *apeglm* package[66]. Functional enrichment analysis was performed on differentially expressed genes by PANTHER overrepresentation Fisher's Exact test and $\log_{10}$ false discovery rates were calculated.

Quantification and statistical analysis

All statistical analysis was performed using Prism® 9.1.0 software (GraphPad). All data were tested for normal (Guassian) distribution using a Shapiro-Wilk normality test. Data presented graphically show mean ± standard error of the mean (SEM) (parametric) or median ± interquartile range (IQR) (non-parametric) unless otherwise indicated in results. Two independent data sets were compared by student's unpaired *t*-test (parametric) or Mann-Whitney test (non-parametric). Paired data were compared using a student's paired *t*-test (parametric) or Wilcoxon matched-pairs signed rank test (non-parametric). Where appropriate, correlation analysis was performed for parametric or non-parametric data using a Pearson's or Spearman's correlation test, respectively. A p-value of <0.05 was considered statistically significant.

References

1. Asrani, S.K., Devarbhavi, H., Eaton, J. and Kamath, P.S. (2019) Burden of liver diseases in the world. J Hepatol. 70(1),151-71.
2. Geneva World Health Organisation 2020 [Available from: https://www.who.int/data/gho/data/themes/mortality-and-global-health-estimates/ghe-leading-causes-of-death.
3. O'Rourke, J.M., Sagar, V.M., Shah, T. and Shetty, S. (2018) Carcinogenesis on the background of liver fibrosis: Implications for the management of hepatocellular cancer. World J Gastroenterol. 24(39), 4436-47.
4. International Agency for Research on Cancer GLOBOCAN 2018 [Available from: https://gco.iarc.fr/today/online-analysis-map?v=2020&mode=population&mode_population=continents&population=900&populations=900&key=asr&sex=0&cancer=11&type=0&statistic=5&prevalence=0&population_group=0&ages_group%5B%5D=0&ages_group%5B%5D=17&nb_items=10&group_cancer=1&include_nmsc=1&include_nmsc_other=1&projection=natural-

earth&color_palette=default&map_scale=quantile&map_nb_colors=5&continent=0&show_ranking=0&rotate=%255B10%252C0%255D.
5. Shetty, S., Lalor, P.F. and Adams, D.H. (2018) Liver sinusoidal endothelial cells - gatekeepers of hepatic immunity. Nat Rev Gastroenterol Hepatol. 15(9), 555-67.
6. Wilkinson, A.L., Qurashi, M. and Shetty, S. (2020) The role of sinusoidal endothelial cells in the axis of inflammation and cancer within the liver. Front Physiol. 11, 990.
7. Niemelä, H., Elima, K., Henttinen, T., Irjala, H., Salmi, M. and Jalkanen, S. (2005) Molecular identification of PAL-E, a widely used endothelial-cell marker. Blood 106(10), 3405-9.
8. Schlingemann, R.O., Dingjan, G.M., Emeis, J.J., Blok, J., Warnaar, S.O. and Ruiter, D.J. (1985) Monoclonal antibody PAL-E specific for endothelium. Lab Invest. 52(1), 71-6.
9. Stan, R.-V., Kubitza, M. and Palade, GE. (1999) PV-1 is a component of the fenestral and stomatal diaphragms in fenestrated endothelia. Proceedings of the National Academy of Sciences. 96(23), 13203.
10. Stan, R.-V., Tse, D., Deharvengt, S.J., Smits, N.C., Xu, Y., Luciano, M.R., McGarry, C.L., Buitendijk, M., Nemani, K.V., Elgueta, R. et al. (2012) The diaphragms of fenestrated endothelia: gatekeepers of vascular permeability and blood composition. Dev Cell. 23(6),1203-18.
11. Herrnberger, L., Seitz, R., Kuespert, S., Bosl, M.R., Fuchshofer, R. and Tamm, E.R. (2012) Lack of endothelial diaphragms in fenestrae and caveolae of mutant Plvap-deficient mice. Histochem Cell Biol. 138(5), 709-24.
12. Keuschnigg, J., Henttinen, T., Auvinen, K., Karikoski, M., Salmi, M. and Jalkanen, S. (2009) The prototype endothelial marker PAL-E is a leukocyte trafficking molecule. Blood. 114(2), 478-84.
13. Rantakari, P., Auvinen, K., Jappinen, N., Kapraali, M., Valtonen, J., Karikoski, M., Gerke, H., Iftakhar-E-Khuda, I., Keuschnigg, J., Umemoto, E. et al. (2015) The endothelial protein PLVAP in lymphatics controls the entry of lymphocytes and antigens into lymph nodes. Nat Immunol. 16(4), 386-96.
14. Rantakari, P., Jappinen, N., Lokka, E., Mokkala, E., Gerke, H., Peuhu, E., Ivaska, J., Elima, K., Auvinen, K. and Salmi, M. (2016) Fetal liver endothelium regulates the seeding of tissue-resident macrophages. Nature 538(7625):392-6.
15. Ramachandran, P., Dobie, R., Wilson-Kanamori, J.R., Dora, E.F., Henderson, B.E.P., Luu, N.T., Portman, J.R., Matchett, K.P., Brice, M., Marwick, J.A. et al. (2019) Resolving the fibrotic niche of human liver cirrhosis at single-cell level. Nature. 575(7783), 512-8.
16. Sharma, A., Seow, J.J.W., Dutertre, C.-A., Pai, R., Blériot, C., Mishra, A., Wong, R.M.M., Singh, G.S.N., Sudhagar, S., Khalilnezhad S. et al. (2020) Onco-fetal Reprogramming of Endothelial Cells Drives Immunosuppressive Macrophages in Hepatocellular Carcinoma. Cell. 183(2), 377-94.e21.
17. Ferreira-Gonzalez, S., Rodrigo-Torres, D., Gadd, V.L., Forbes, S.J. (2021) Cellular Senescence in Liver Disease and Regeneration. Semin Liver Dis. 41(1), 50-66.
18. Hoare, M. and Narita, M. (2018) The Power Behind the Throne: Senescence and the Hallmarks of Cancer. Ann Rev Cancer Biol. 2(1),175-94.
19. Kang, T.-W., Yevsa, T., Woller, N., Hoenicke, L., Wuestefeld, T., Dauch, D., Hohmeyer, A., Gereke, M., Rudalska, R., Potapova A. et al. (2011) Senescence surveillance of pre-malignant hepatocytes limits liver cancer development. Nature. 479(7374), 547-51.
20. Eggert, T., Wolter, K., Ji, J., Ma, C., Yevsa, T., Klotz, S., Medina-Echeverz, J., Longerich, T., Forgues, M., Reisinger, F. et al. (2016) Distinct Functions of Senescence-Associated Immune Responses in Liver Tumor Surveillance and Tumor Progression. Cancer Cell. 30(4), 533-47.
21. Hoare, M., Ito, Y., Kang, T.-W., Weekes, M.P., Matheson, N.J., Patten, D.A., Shetty, S., Parry, A.J., Menon, S., Salama, R. et al. (2016) NOTCH1 mediates a switch between two distinct secretomes during senescence. Nat Cell Biol. 18(9), 979-92.
22. Crary GS and Albrecht JH. (1998) Expression of cyclin-dependent kinase inhibitor p21 in human liver. Hepatology. 28(3), 738-43.
23. Lunz III, J.G., Tsuji, H., Nozaki, I., Murase, N. and Demetris, A.J. (2005) An inhibitor of cyclin-dependent kinase, stress-induced p21Waf-1/Cip-1, mediates hepatocyte mito-inhibition during the evolution of cirrhosis. Hepatology. 41(6), 1262-71.
24. Aravinthan, A., Scarpini, C., Tachtatzis, P., Verma, S., Penrhyn-Lowe, S., Harvey, R., Davies, S.E., Allison, M., Coleman, N., and Alexander, G. (2013) Hepatocyte senescence predicts progression in non-alcohol-related fatty liver disease. J Hepatol. 58(3), 549-56.

25. Wan, Y., McDaniel, K., Wu, N., Ramos-Lorenzo, S., Glaser, T., Venter, J., Francis, H., Kennedy, L., Sato, K., Zhou, T. et al. (2017) Regulation of Cellular Senescence by miR-34a in Alcoholic Liver Injury. Am J Pathol. 187(12), 2788-98.
26. Acosta, J.C., Banito, A., Wuestefeld, T., Georgilis, A., Janich, P., Morton, J.P., Athineos, D., Kang, T.-W., Lasitschka, F., Andrulis, M. et al. (2013) A complex secretory program orchestrated by the inflammasome controls paracrine senescence. Nat Cell Biol. 15(8), 978-90.
27. Bardadin, K.A., Scheuer, P.J., Peczek, A. and Wejman, J. (1991) Immunocytochemical observations on macrophage populations in normal fetal and adult human liver. J Pathol. 164(3), 253-9.
28. McGuinness, P.H., Painter, D., Davies, S. and McCaughan, G.W. (2000) Increases in intrahepatic CD68 positive cells, MAC387 positive cells, and proinflammatory cytokines (particularly interleukin 18) in chronic hepatitis C infection. Gut. 46(2), 260.
29. Soulas, C., Conerly, C., Kim, W.-K., Burdo, T.H., Alvarez, X., Lackner, A.A. and Williams, K.C. (2011) Recently infiltrating MAC387(+) monocytes/macrophages a third macrophage population involved in SIV and HIV encephalitic lesion formation. Am J Pathol. 178(5), 2121-35.
30. Lalor, P.F., Edwards, S., McNab, G., Salmi, M., Jalkanen, S. and Adams, D.H. (2002) Vascular adhesion protein-1 mediates adhesion and transmigration of lymphocytes on human hepatic endothelial cells. J Immunol. 169(2), 983-92.
31. Strickland, L.A., Jubb, A.M., Hongo, J.A., Zhong, F., Burwick, J., Fu, L., Frantz, G.D. and Koeppen, H. (2005) Plasmalemmal vesicle-associated protein (PLVAP) is expressed by tumour endothelium and is upregulated by vascular endothelial growth factor-A (VEGF). J Pathol. 206(4), 466-75.
32. Bodor, C., Nagy, J.P., Végh, B., Németh, A., Jenei, A., MirzaHosseini, S., Sebe, A. and Rosivall, L. (2012) Angiotensin II increases the permeability and PV-1 expression of endothelial cells. Am J Physiol-Cell Physiol. 302(1), C267-C76.
33. Carson-Walter, E.B., Hampton, J., Shue, E., Geynisman, D.M., Pillai, P.K., Sathanoori, R., Madden, S.L., Hamilton, R.L. and Walter, K.A. (2005) Plasmalemmal vesicle associated protein-1 is a novel marker implicated in brain tumor angiogenesis. Clin Cancer Res. 11(21), 7643-50.
34. Kim, S.A., Kim, S.J., Choi, Y.A., Yoon, H.-J., Kim, A. and Lee, J. (2020) Retinal VEGFA maintains the ultrastructure and function of choriocapillaris by preserving the endothelial PLVAP. Biochem Biophys Res Commun. 522(1), 240-6.
35. Hamilton, B.J., Tse, D. and Stan, R.V. (2019) Phorbol esters induce PLVAP expression via VEGF and additional secreted molecules in MEK 1-dependent and p38, JNK and PI 3K/Akt-independent manner. J Cell Mol Med. 23(2), 920-33.
36. Bocca, C., Novo, E., Miglietta, A. and Parola, M. (2015) Angiogenesis and Fibrogenesis in Chronic Liver Diseases. Cell Mol Gastroenterol Hepatol. 1(5), 477-88.
37. Morse, M.A., Sun, W., Kim, R., He, A.R., Abada, P.B., Mynderse, M. and Finn, R.S. (2019) The Role of Angiogenesis in Hepatocellular Carcinoma. Clin Cancer Res. 25(3), 912-20.
38. Ishikawa, K., Mochida, S., Mashiba, S., Inao, M., Matsui, A., Ikeda, H., et al. (1999) Expressions of vascular endothelial growth factor in nonparenchymal as well as parenchymal cells in rat liver after necrosis. Biochem Biophys Res Commun. 254(3), 587-93.
39. Archambault, A.-J., Sirois, M.G., Bernatchez, P.N., Fiset, C. and Haddad, P.S. (2001) Vascular endothelial growth factor production by isolated rat hepatocytes after cold ischemia—warm reoxygenation. Liver Transpl. 7(11), 988-97.
40. Donahower, B., McCullough, S.S., Kurten, R., Lamps, L.W., Simpson, P., Hinson, J.A. and James, L.P. (2006) Vascular endothelial growth factor and hepatocyte regeneration in acetaminophen toxicity. Am J Physiol-Gastrointest Liver Physiol. 291(1), G102-G9.
41. Yin, K., Patten, D.A., Gough, S., de Barros Goncalves, S., Chan, A., Olan, I., Cassidy, L., Poblocka, M., Zhu, H., Lun, A. et al. (2022) Senescence-induced endothelial phenotypes underpin immune-mediated senescence surveillance. Genes Dev. 36(9-10), 533-49.
42. Shetty, S., Weston, C.J., Adams, D.H. and Lalor, P.F. (2014) A flow adhesion assay to study leucocyte recruitment to human hepatic sinusoidal endothelium under conditions of shear stress. J Vis Exp. (85).
43. Shetty, S., Bruns, T., Weston, C.J., Stamataki, Z., Oo, Y.H., Long, H.M., Reynolds, G.M., Pratt, G., Moss, P., Jalkanen, S. et al. (2012) Recruitment mechanisms of primary and malignant B cells to the human liver. Hepatology. 56(4), 1521-31.

44. Shetty, S., Weston, C.J., Oo, Y.H., Westerlund, N., Stamataki, Z., Youster, J., Hubscher, S.G., Salmi, M., Jalkanen, S., Lalor, P.F. et al. (2011) Common lymphatic endothelial and vascular endothelial receptor-1 mediates the transmigration of regulatory T cells across human hepatic sinusoidal endothelium. J Immunol. 186(7), 4147-55.
45. Escribano, J., Chen, M.B., Moeendarbary, E., Cao, X., Shenoy, V., Garcia-Aznar, J.M., Kamm, R.D. and Spill, F. (2019) Balance of mechanical forces drives endothelial gap formation and may facilitate cancer and immune-cell extravasation. PLoS Comput Biol. 15(5), e1006395.
46. Nakagami, Y., Hatano, E., Chayama, Y. and Inoue, T. (2019) An anti-PLVAP antibody suppresses laser-induced choroidal neovascularization in monkeys. Eur J Pharmacol. 854, 240-6.
47. Stan, R.V., Tkachenko, E. and Niesman, I.R. (2004) PV1 is a key structural component for the formation of the stomatal and fenestral diaphragms. Mol Biol Cell. 15(8),3615-30.
48. Wasserman, S.M., Mehraban, F., Komuves, L.G., Yang, R.-B., Tomlinson, J.E., Zhang, Y., Spriggs, F. and Topper, J.N. (2002) Gene expression profile of human endothelial cells exposed to sustained fluid shear stress. Physiol Genomics. 12(1), 13-23.
49. Desroches-Castan, A., Tillet, E., Ricard, N., Ouarne, M., Mallet, C., Belmudes, L., Couté, Y., Boillot, O., Scoazec, J.Y., Bailly, S. et al. (2019) Bone Morphogenetic Protein 9 Is a Paracrine Factor Controlling Liver Sinusoidal Endothelial Cell Fenestration and Protecting Against Hepatic Fibrosis. Hepatology. 70(4), 1392-408.
50. Muradashvili, N., Benton, R.L., Tyagi, R., Tyagi, S.C. and Lominadze, D. (2014) Elevated level of fibrinogen increases caveolae formation; Role of matrix metalloproteinase-9. Cell Biochem Biophys. 69(2), 283-94.
51. Patten, D.A., Wilson, G.K., Bailey, D., Shaw, R.K., Jalkanen, S., Salmi, M., Rot, A., Weston, C.J., Adams, D.H. and Shetty, S. (2017) Human liver sinusoidal endothelial cells promote intracellular crawling of lymphocytes during recruitment: A new step in migration. Hepatology. 65(1), 294-309.
52. Liu, P., Tang, Q., Chen, M., Chen, W., Lu, Y., Liu, Z., and He, Z. (2020) Hepatocellular Senescence: Immunosurveillance and Future Senescence-Induced Therapy in Hepatocellular Carcinoma. Front Oncol. 10.
53. Bird, T.G, Müller, M., Boulter, L., Vincent,, D.F., Ridgway, R.A., Lopez-Guadamillas, E., Lu, W.Y., Jamieson, T., Govaere, O., Campbell, A.D. et al. (2018) TGFβ inhibition restores a regenerative response in acute liver injury by suppressing paracrine senescence. Sci Transl Med. 10(454), eaan1230.
54. Ferreira-Gonzalez, S., Lu, W.-Y., Raven, A., Dwyer, B., Man, T.Y., O'Duibhir, E., Lewis, P.J.S., Campana, L., Kendall, T.J., Bird, T.G. et al. (2018) Paracrine cellular senescence exacerbates biliary injury and impairs regeneration. Nat Commun. 9(1), 1020.
55. Holt, A.P., Salmon, M., Buckley, C.D. and Adams, D.H. (2008) Immune interactions in hepatic fibrosis. Clinics Liver Dis.12(4), 861.
56. Heemskerk N, Schimmel L, Oort C, van Rijssel J, Yin T, Ma B, Van Unen, J., Pitter, B., Huveneers, S., Goedhart, J. et al. (2016) F-actin-rich contractile endothelial pores prevent vascular leakage during leukocyte diapedesis through local RhoA signalling. Nat Commun. 7(1), 10493.
57. Patten, D.A., Kamarajah, S.K., Rose, J.M., Tickle, J., Shepherd, E.L., Adams, D.H., Weston, C.J. and Shetty, S. (2017) SCARF-1 promotes adhesion of $CD4^+$ T cells to human hepatic sinusoidal endothelium under conditions of shear stress. Sci Rep. 7(1):1-15.
58. Arts, J.J., Mahlandt, E.K., Grönloh, M.L., Schimmel, L., Noordstra, I., Gordon, E., van Steen, A.C., Tol, S., Walzog, B., van Rijssel, J. et al. (2021) Endothelial junctional membrane protrusions serve as hotspots for neutrophil transmigration. eLife. 10, e66074.
59. Iwakiri, Y., Shah, V., Rockey, D.C. (2014) Vascular pathobiology in chronic liver disease and cirrhosis - current status and future directions. J Hepatol. 61(4), 912-24.
60. Tacke, F. and Zimmermann, H.W. (2014) Macrophage heterogeneity in liver injury and fibrosis. J Hepatol. 60(5), 1090-6.
61. Holt, A.P., Haughton, E.L., Lalor, P.F., Filer, A., Buckley, C.D. and Adams, D.H. (2009) Liver myofibroblasts regulate infiltration and positioning of lymphocytes in human liver. Gastroenterol. 136(2), 705-14.
62. Arthur, M.J., Friedman, S.L., Roll, F.J. and Bissell, D.M. (1989) Lipocytes from normal rat liver release a neutral metalloproteinase that degrades basement membrane (type IV) collagen. J Clin Invest. 84(4),1076-85.

63. Patro, R., Duggal, G., Love, M.I., Irizarry, R.A. and Kingsford, C. (2017) Salmon provides fast and bias-aware quantification of transcript expression. Nature methods. 14(4), 417-9.
64. Soneson, C., Love, M.I. and Robinson, M.D. (2015) Differential analyses for RNA-seq: transcript-level estimates improve gene-level inferences. F1000Research. 4.
65. Love, M.I., Anders, S. and Huber, W. (2017) Analyzing RNA-seq data with DESeq2. Bioconductor. 2, 1-63.
66. Zhu, A., Ibrahim, J.G. and Love, M.I. (2019) Heavy-tailed prior distributions for sequence count data: removing the noise and preserving large differences. Bioinformatics. 35(12), 2084-92.

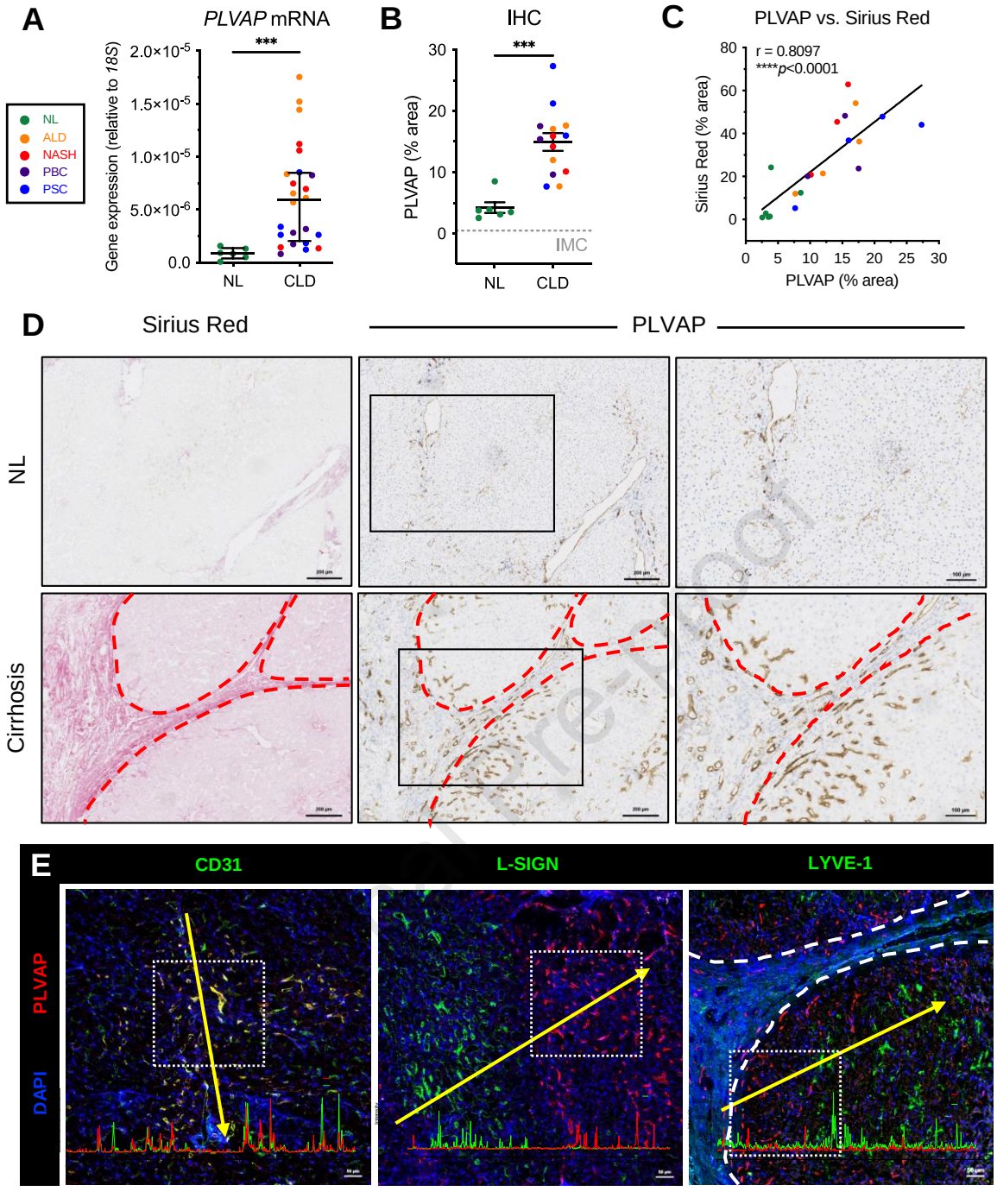
A
PLVAP mRNA
***
Gene expression (relative to 18S)
2.0×10-5
1.5×10-5
1.0×10-5
5.0×10-6
0.0
NL
CLD
NL
ALD
NASH
PBC
PSC
B
IHC
***
PLVAP (% area)
30
20
10
0
IMC
NL
CLD
C
PLVAP vs. Sirius Red
r = 0.8097
****p<0.0001
Sirius Red (% area)
80
60
40
20
0
0 5 10 15 20 25 30
PLVAP (% area)
D
Sirius Red
PLVAP
NL
Cirrhosis
E
CD31
L-SIGN
LYVE-1
PLVAP
DAPI

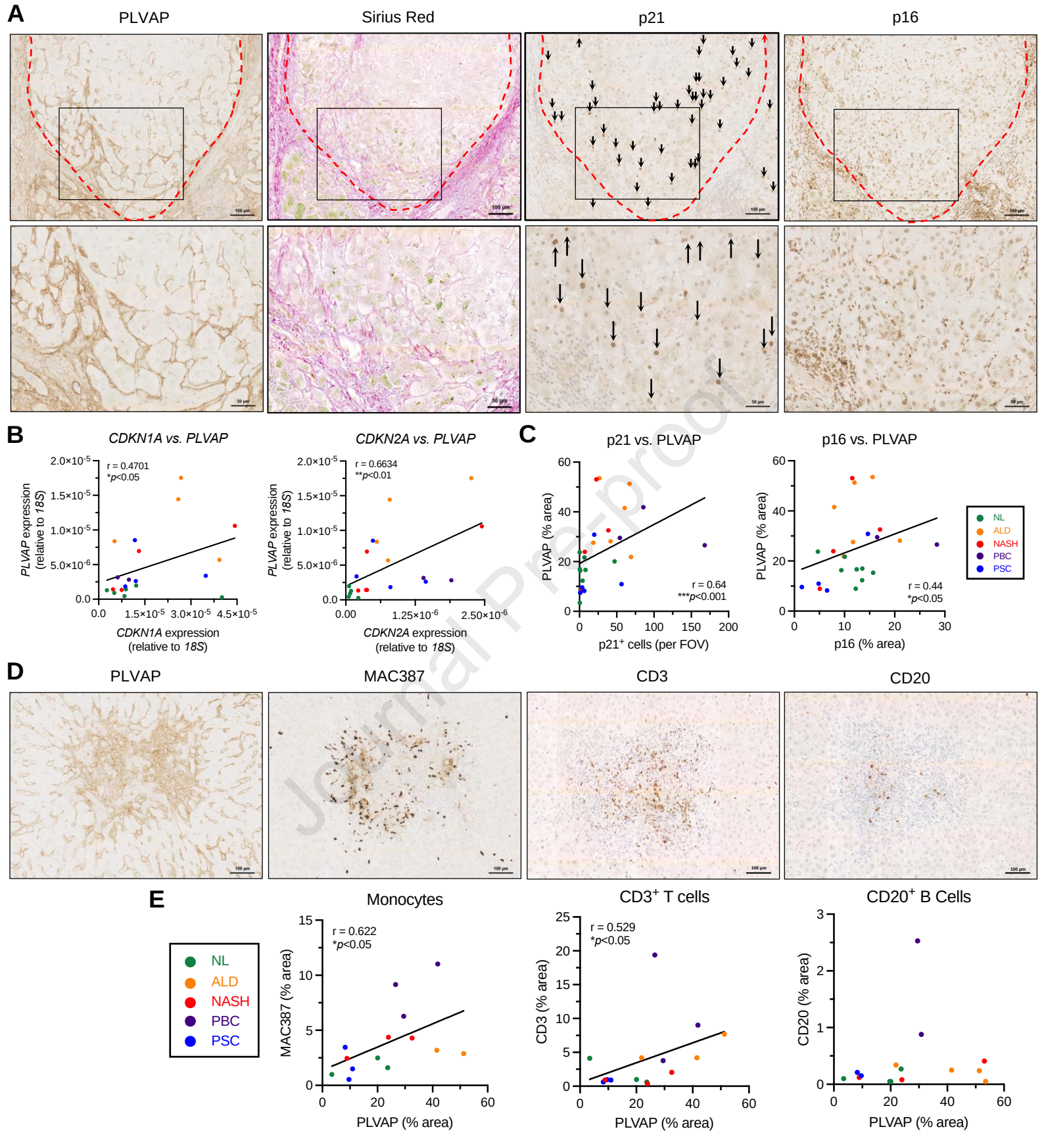

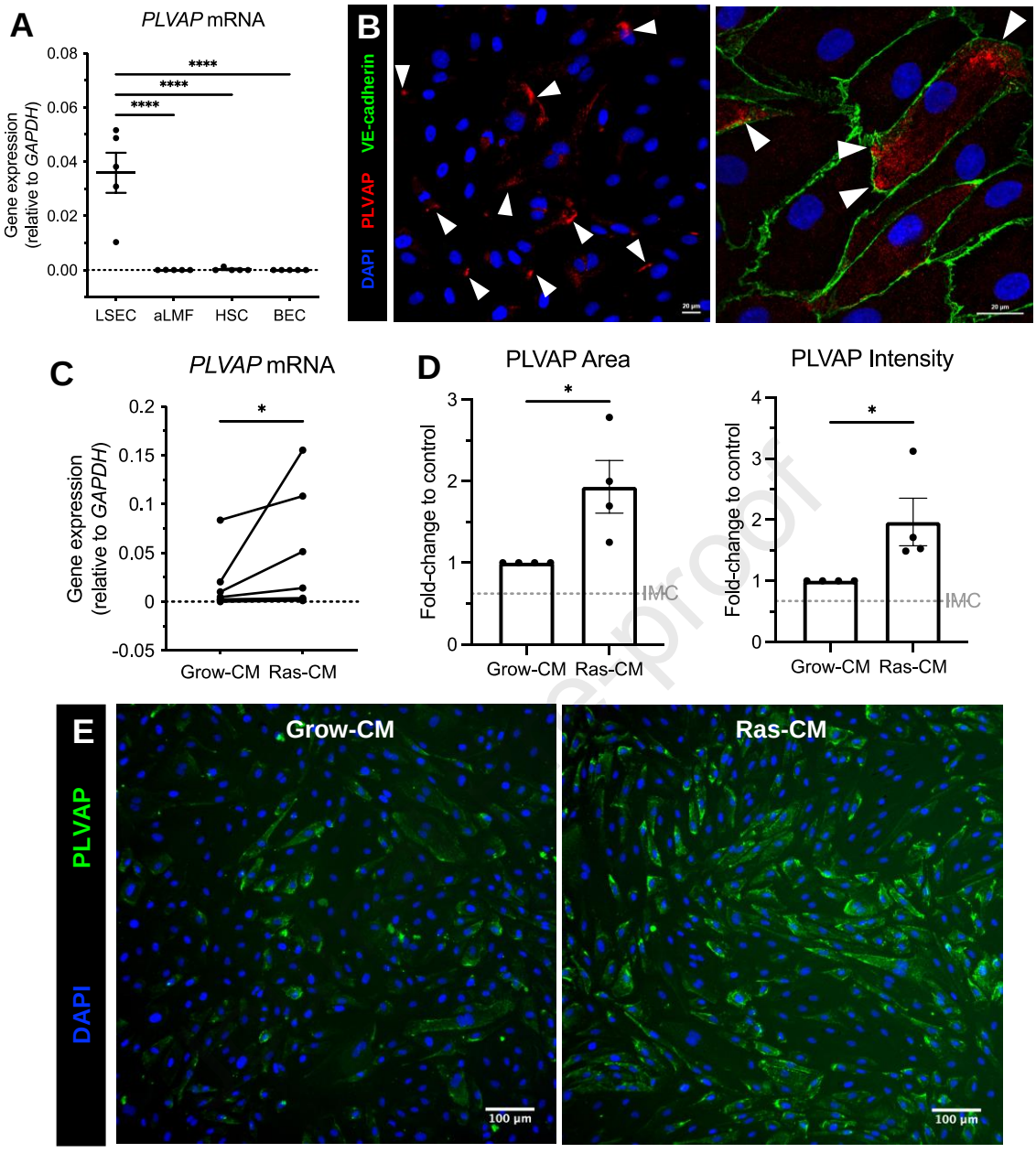
A
PLVAP mRNA
Gene expression (relative to GAPDH)
0.08
0.06
0.04
0.02
0.00
****
****
****
LSEC
aLMF
HSC
BEC
B
DAPI
PLVAP
VE-cadherin
C
PLVAP mRNA
Gene expression (relative to GAPDH)
0.2
0.15
0.1
0.05
0
-0.05
*
Grow-CM
Ras-CM
D
PLVAP Area
Fold-change to control
3
2
1
0
*
IMC
Grow-CM
Ras-CM
PLVAP Intensity
Fold-change to control
4
3
2
1
0
*
IMC
Grow-CM
Ras-CM
E
PLVAP
DAPI
Grow-CM
Ras-CM
100 µm
100 µm

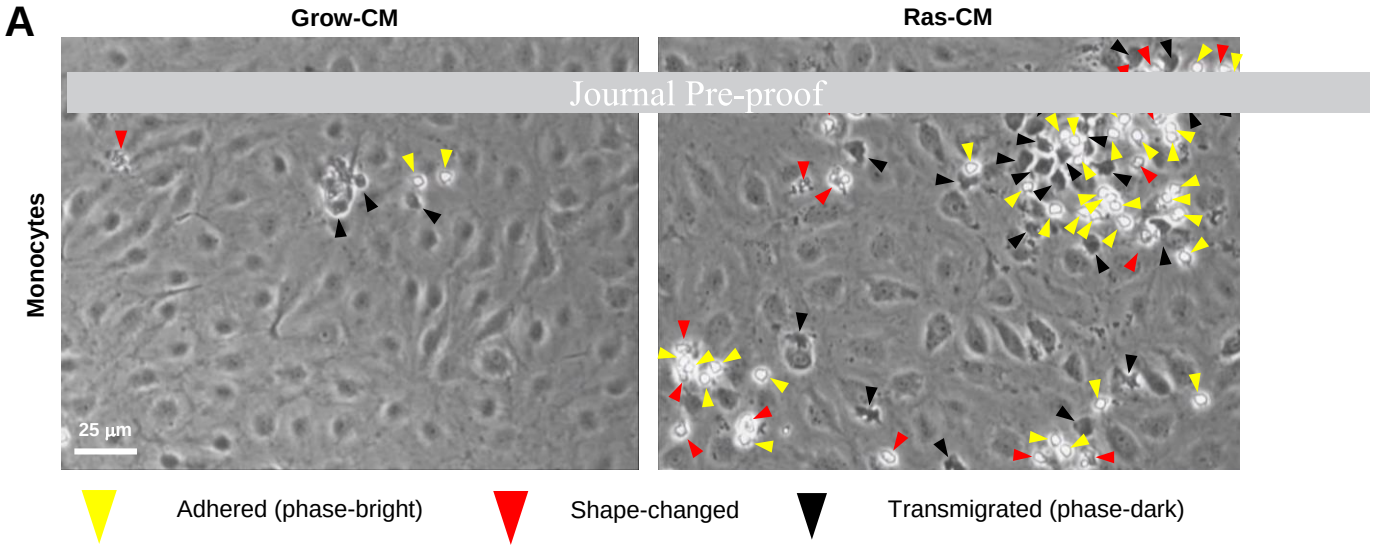

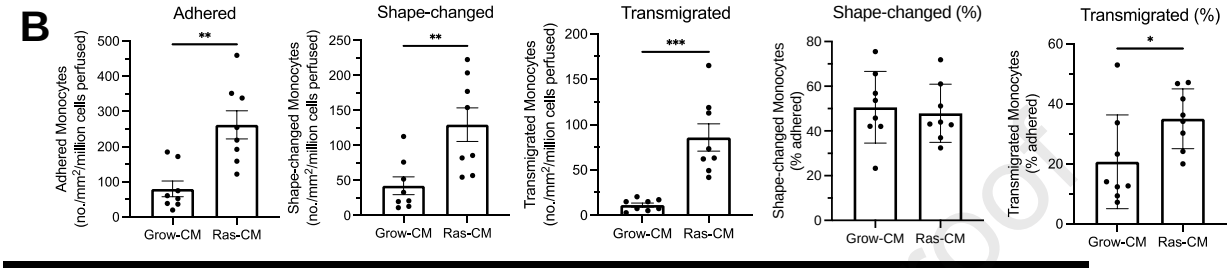

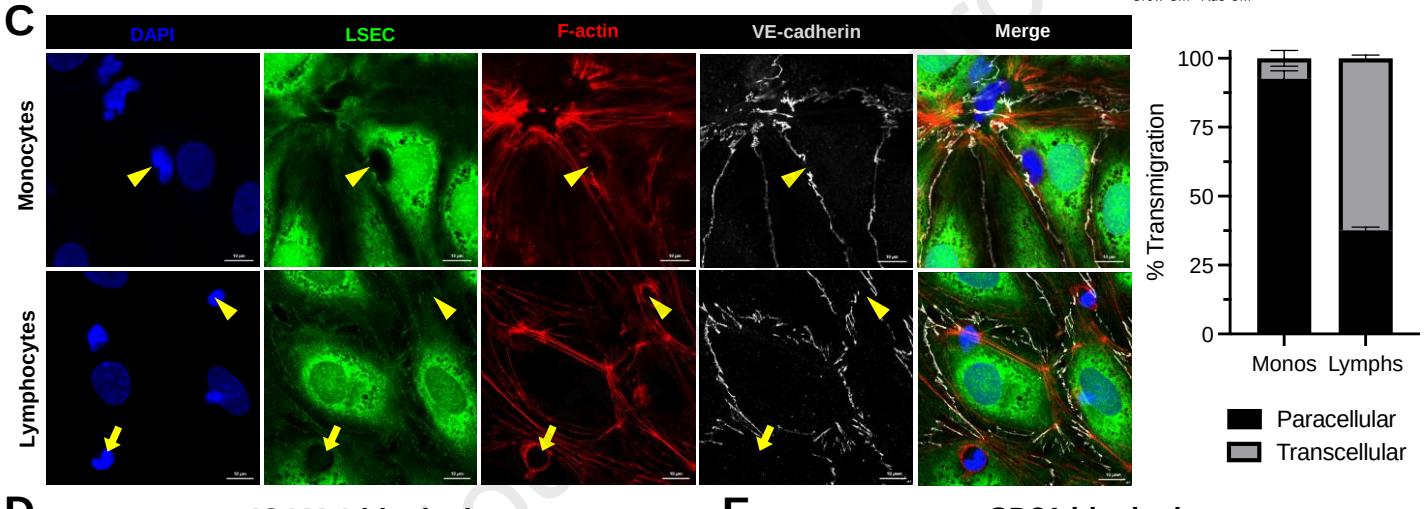

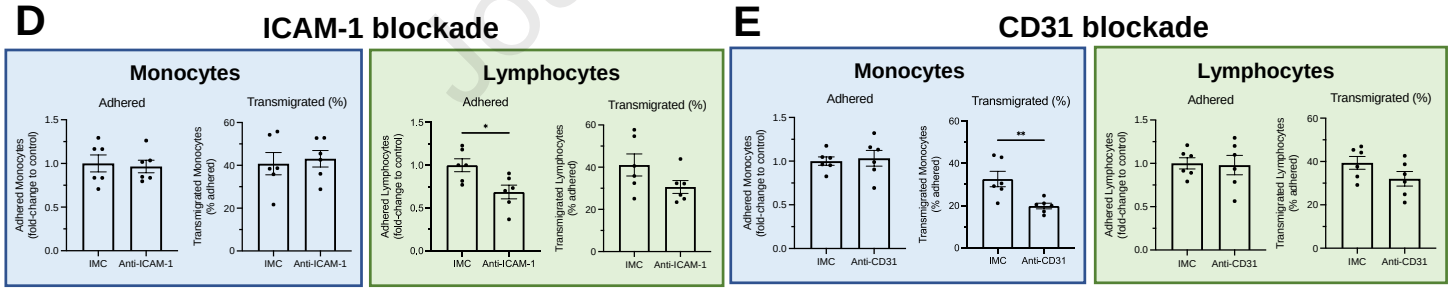

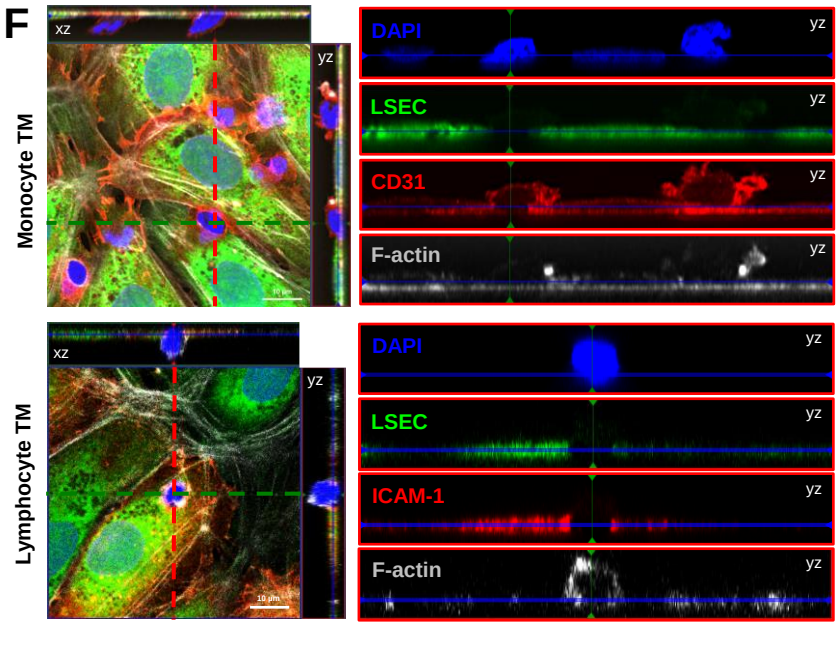

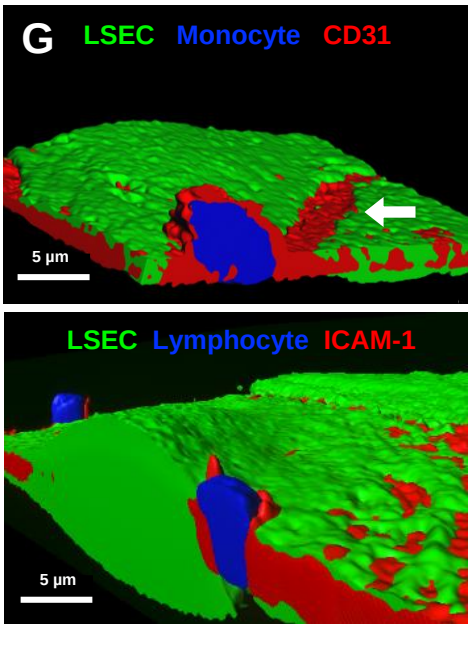

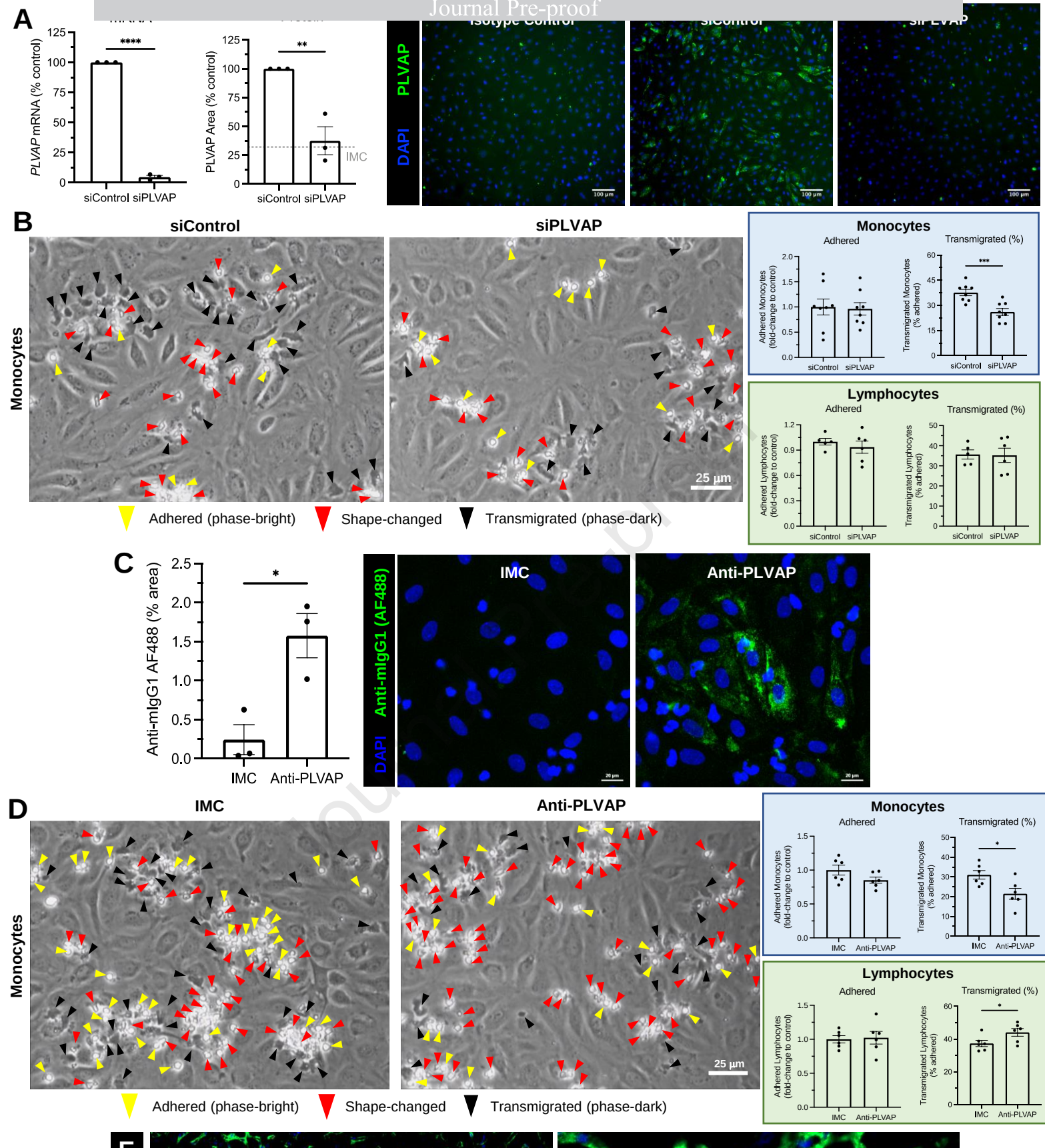

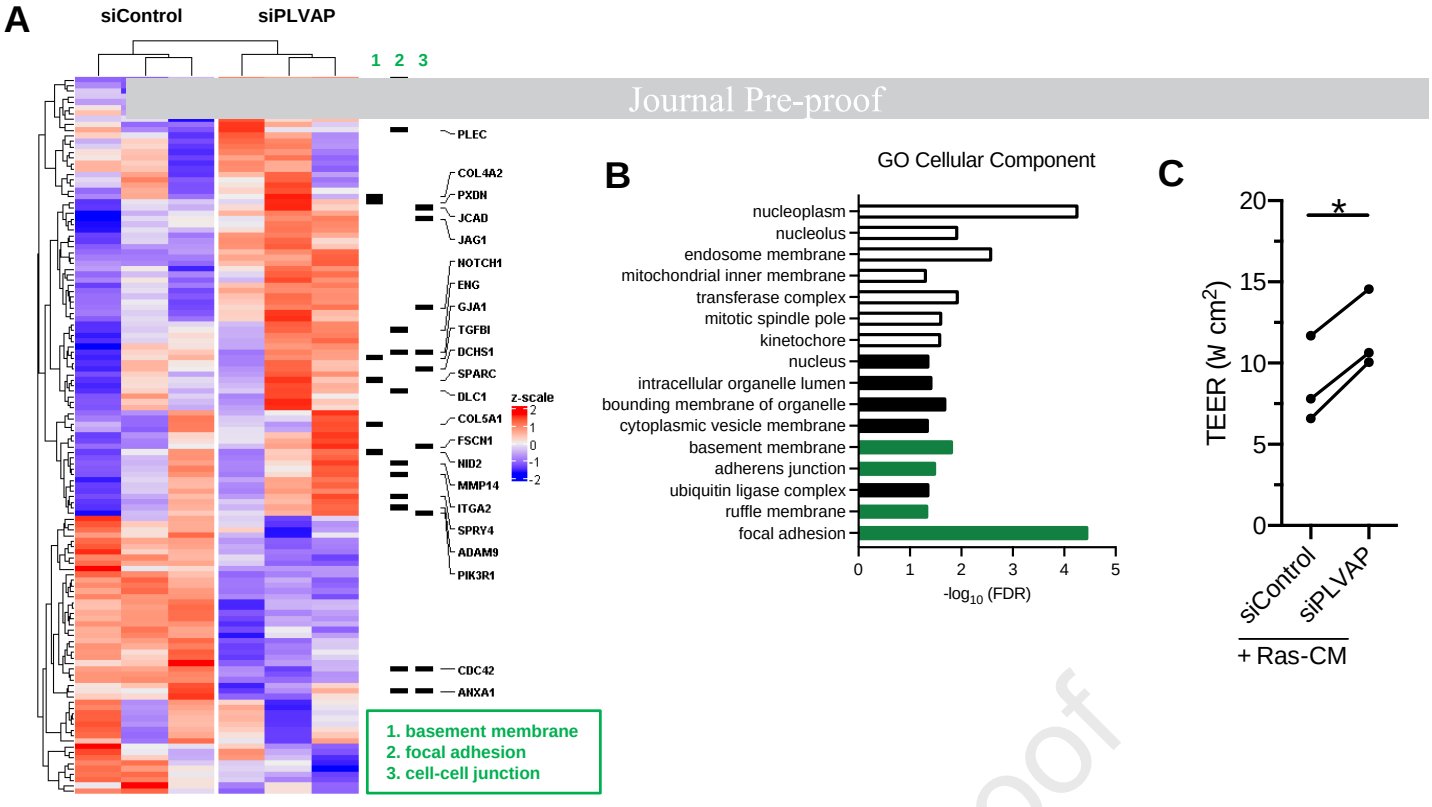

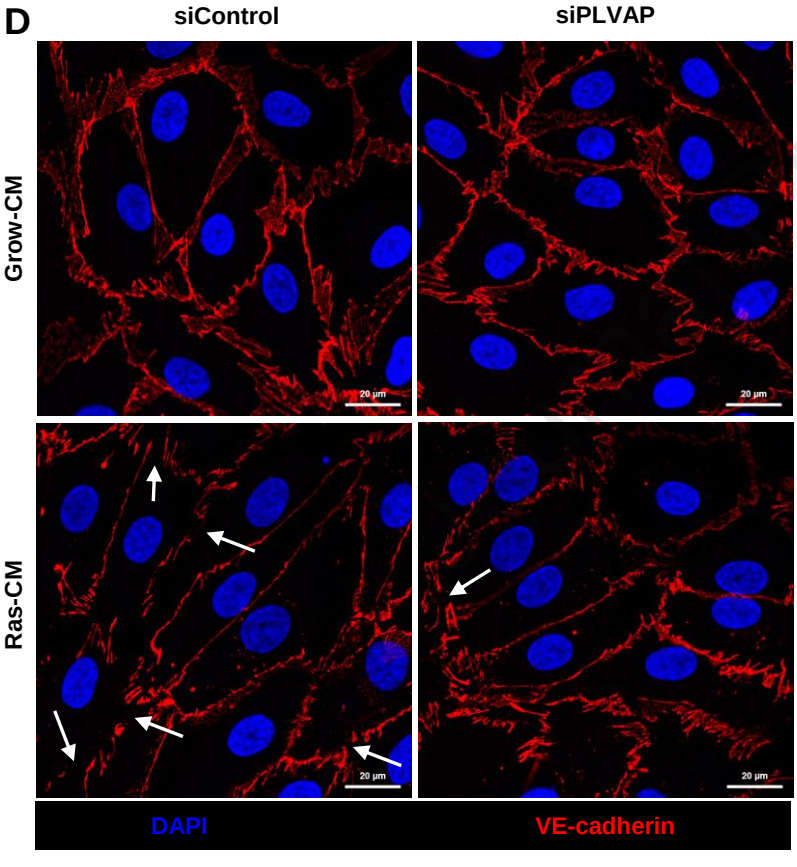

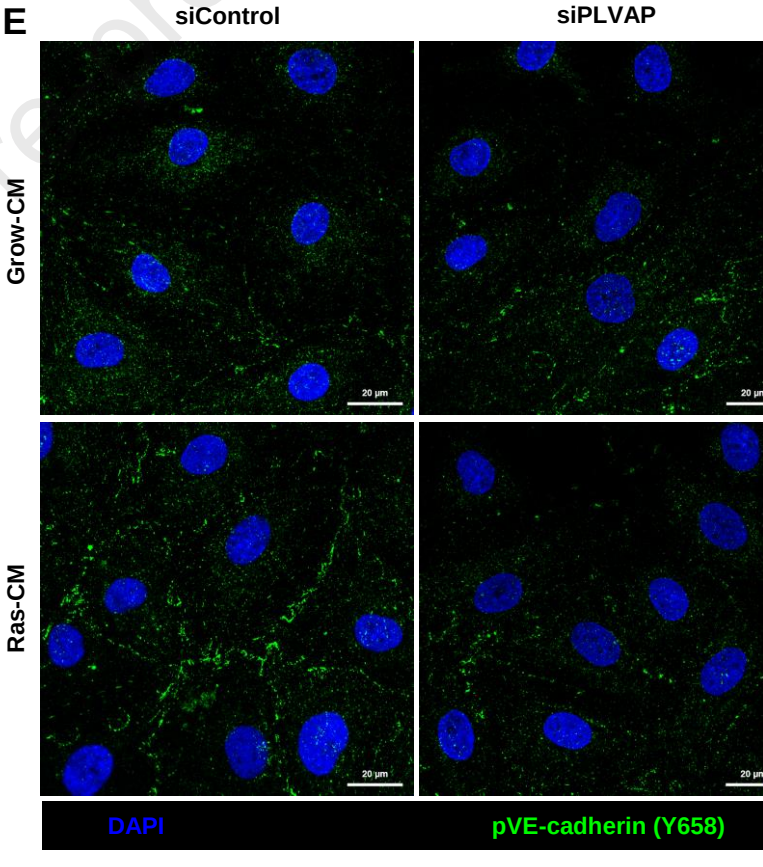

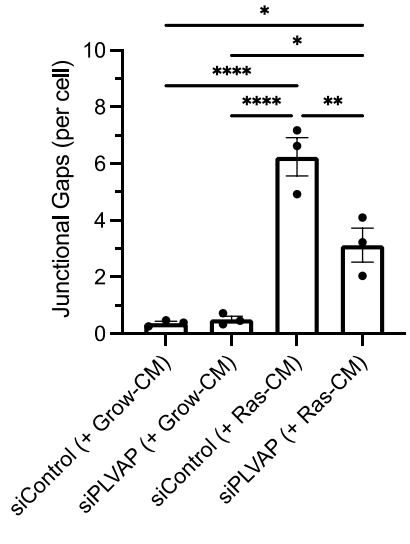

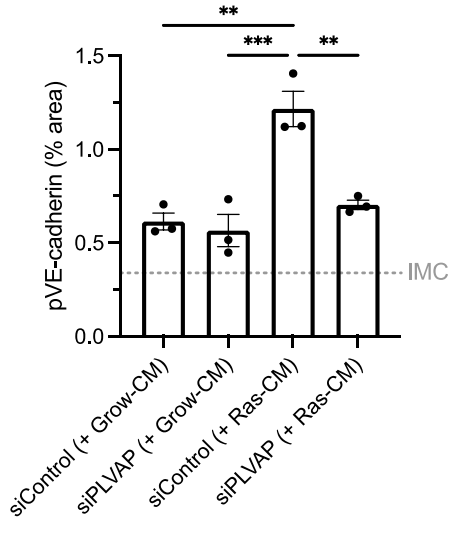

Highlights

PLVAP expression in human liver disease correlates with markers of tissue senescence.

Human liver endothelium upregulates PLVAP when exposed to the SASP *in vitro*.

PLVAP mediates endothelial barrier function by regulating phospho-VE Cadherin levels.

PLVAP supports paracellular transmigration of monocytes in SASP treated endothelium.